Analysis of aerosol particles for the determination of energy losses in solar power plants

Thesis of: Juan Prats Briceño

Study course: Mechanical Engineering

Major topic: Solar energy

Saragossa, October 2012

This thesis was supervised by:

Mr. Dr. rer. nat. Markus Sauerborn

Solar-Institut Jülich

Fachhochschule Aachen

Mr. Prof. Dr.-Ing. Cristobal Cortés

Energy department

Universidad de Zaragoza

This thesis was written independently.

There was no other literature used
except the mentioned ones.

Saragossa, the 02.10.2012

Acknowledgments

FH AACHEN
UNIVERSITY OF APPLIED SCIENCES

Abstract

This thesis is a study about the influence of the aerosol particles on the circumsolar radiation. The research started in October 2011 with the reading and learning about other studies on the CSR and aerosol particles. It was also necessary study the functioning of the devices, which were going to be used. For each machine it took about one week to understand how it worked and they were then tested one by one. In December 2011, once some initial problems had been solved, the measurements could finally start to be taken, and by the end of January all of the data was recorded. The calculations and the literature work has been done in the city of Saragossa, Spain, since February 2012 until October 2012.

Table of contents

FH AACHEN
UNIVERSITY OF APPLIED SCIENCES

Analysis of aerosol particles for the determination of energy losses in solar power plants

1 Introduction and goals

This thesis was written for the "Solar-Institut Jülich" (SIJ), located in Jülich, Germany. The SIJ was founded in 1992 as a scientific institution of the university of applied sciences "FH Aachen". The aim of the institute is the research and development in the field of renewable energy, especially in solar energy. One of the most important projects in which the SIJ participates, is the "Solarturm Jülich" (STJ). The STJ is a high temperature solar thermal power plant. It has an absorber on the top of the tower, which receives the solar radiation reflected by 2150 heliostat. The absorber is made of ceramic and it transmits the solar radiation to the working fluid, air in this case, to a temperature of 700ºC. This air heats steam and it works in a steam turbine to generate as maximum 1500 KW. /1/

This kind of high temperature solar thermal power plant can have an efficiency of about 17%. Losses that are normally considered are, for example, due to the wind, cosines losses, reflexion or absorption /2/. But there also are losses, which are disregarded and this thesis is going to be focused one of these losses. The aerosol particles in the air of the atmosphere can scatter the solar radiation, deviating its direction slightly. This causes what is known as circumsolar radiation, which is still measured as direct radiation (the incoming energy in a high temperature solar thermal power plant), but it reaches the absorber offering a more divergent beam with less concentration.

For this thesis, four different devices have been used: a ceilometer, an aerosol spectrometer, a weather station and a CCD camera. The ceilometer is a meteorologic instrument using reflected laser light to measure cloud and the particles layers in the atmosphere from the ground level up to a height of 15000 m. With the aerosol spectrometer the concentration and size of aerosol particles on the ground level can be measured. The weather station of the SIJ is made up of many different devices. The most important ones being the pyrheliometer and the pyranometer, which are used to measure the direct radiation and the global radiation. Finally, a CCD camera with a higher resolution (5 megapixel) was used: it was connected to a computer, where the pictures were recorded and analysed by a program. A telephoto lens, a filter and an automatic tripod were used to take the photos. The pictures were then measured with software in order to calculate the radiation coming from the circumsolar area. These measurements were taken on five different days, in eight different moments. Once these measurements had been taken, they were compared and analysed in order to see whether there was any influence of the aerosol particles on the circumsolar radiation or not. The figure 1 shows the place where the measurements were

taken. The majority of the devices were located on the flat roof of the "Naturwissenschaft" building of the SIJ (Jülich, Germany). One can see the camera with the telephoto lens and the linked computer in the foreground. The ceilometer is located in the background on the left and the aerosol spectrometer next to it. The pyrheliometer and the pyranometer cannot be seen in the photo, but they were just a few meters up fixed on a solar tracker.

Figure 1: Place on the institute flat roof where the measurements were taken, in Jülich, Germany

The thesis is divided in 4 big parts and in 9 different chapters. The first part explains the necessary theoretical details in order to understand the thesis. It includes the chapters Solar Radiation, CSR, Aerosol Particles and Clouds. The second part describes how the different devices used in this thesis work and also specifies their technical characteristics. It is divided up in the chapters CHM 15K, Fidas 200, Weather Station and Camera. The third part includes the chapter concerning the measurements, in which all of the results are first listed and then compared. The last part consists of the appendix, in which the calculations are shown in detail.

2 Solar Radiation

2.1 Solar energy:

The sun is a huge sphere composed of high temperature gases. The diameter of the sun is 1.39×10^{9} m /3/ and it is situated $1.49588707 \times 10^{11}$ m from the earth; this distance is called Astronomical Unit (AU). /4/

The sun generates its energy by nuclear fusion reactions, which are produced in the nucleus. So the energy come from the mass loss of the sun, given by the equation $E = m c^{2}$.

The solar nucleus covers 15% of the volume of the entire sun, but it makes up about 40% of the total weight and generates 90% of the energy. The density in the nucleus is approximately 10^{5} kg/m3 and its temperature can reach 10^{7} K. The photosphere, which is the outer layer of the sun, has a radius making up approximately 30% of the entire sun's radius. It is estimated that the temperature in the photosphere is the "effective temperature of the black body", which is 5762 K, and the density is below 10^{5} kg /m3. The photosphere is considered the surface of the sun because it is an opaque region, where the largest part of radiation is emitted to space. /5/

Three factors determine the luminous flux coming from the sun towards the earth: the distance between the sun and the earth, the solar diameter and the temperature of the sun.

The flux emitted by the sun is in engineering usually considered as a constant. Meteorological changes influence the flux in much greater ways than the variation in solar radiation coursed by the changing distance to the sun on the elliptic way around the sun.

The solar constant (G) is the value of the energy flux coming from the sun. A flux is something that passes through a surface, in this case, energy per second. The unit W/m^{2} is thus used. G measures the value of the perpendicular solar incident flux to a surface, G is valid out of earth's atmosphere, when the solar radiation reaches the atmosphere it suffers changes.

The energy flux emitted by a black body (surface of the sun) is given by the Stefan-Boltzmann law. This law states that the energy radiated by a black body is directly proportional to the fourth power of the black body's temperature. In order to calculate the solar constant, the energy flux emitted by the sun is multiplied by the relation of the areas between the sun's surface (rs) and a sphere located at one astronomical unit (ao) to the sun.

Teff is the value of sun's surface temperature (black body's temperature). In the equation 1 the Stefan-Bolzmann law is used in order to calculate the solar constant.

$$G = \sigma \cdot T_{eff} \cdot \left(\frac{r_s}{a_o}\right)^2 = 1366 \; ^W/_{m^2}$$

Equation 1: Solar constant

σ is the Stefan-Boltzmann constant and is derived from others constants of nature. Its value is:

$$\sigma = \frac{2\pi^5 k^5}{15 c^2 h^3} = 5.67073 \times 10^{-8} Js^{-1} m^{-2} K^{-4}$$

Equation 2: Stefan-Boltzmann constant /6/

Since the earth's orbit is elliptical, the astronomical unit is the average of the distance between the sun and the earth throughout the whole year. There is a fluctuation of about 7% of the solar irradiance between the closest point and the farthest. /7/ In this thesis this fluctuation was taken into account.

This constant is valid outside of the atmosphere and in perpendicular direction, so it varies depending on the location's latitude and the atmospheric conditions.

2.2 Spectral distribution of the solar radiation

The sun emits radiation over the whole electromagnetic spectrum, which is divided in ultraviolet (UV), visible and infrared (IR) light. The figure 2 shows how the visible and infrared light have a greater spectral irradiance than the ultraviolet light, so the light with wavelengths bigger than 400 nanometres are the most important to consider in solar energy. The following diagram shows the relation between spectral irradiation and the wavelengths, differentiating between the irradiance at the top of the atmosphere and that at sea level.
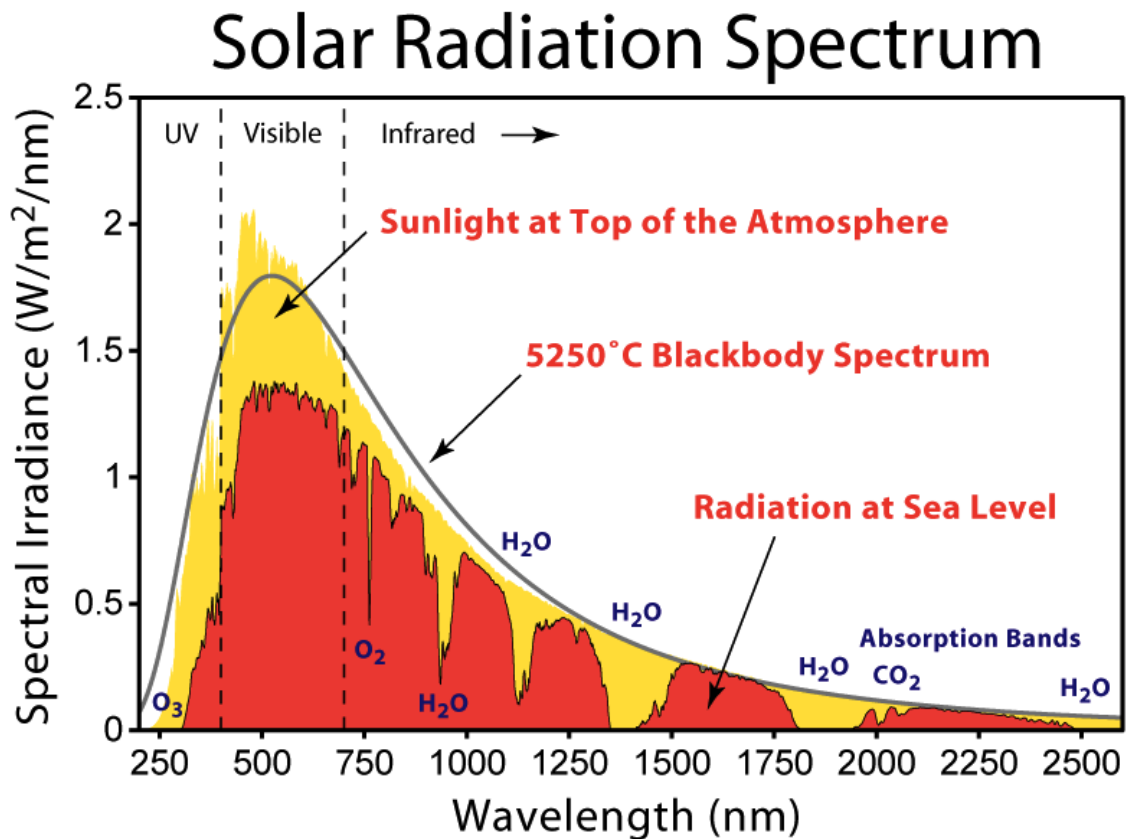
Figure 2: Solar radiation Spectrum /8/

2.3 Losses in the atmosphere:

In order to reach to the earth's surface, the solar radiation must pass through the earth's atmosphere, where the radiation might undergo changes. Reflection, absorption and scattering cause these changes in the atmosphere.

The incoming solar radiation can reach the earth ground in three different forms: direct, diffuse and reflected. Direct radiation comes directly from the solar sphere and it is the one that is going to be useful for solar thermal energy. Diffuse radiation has been scattered before it has reached the surface, for example on a cloudy day. Solar radiation is reflected by the earth surface, so reflected radiation is the direct or diffuse radiation after have been reflected by the earth. The total of all of them is called global radiation.

Absorption and backscattering do not let the radiation get to the atmosphere. A body can absorb part of the impact energy and it can also reflect it back to the space, which is called backscattering. These phenomenons occur due to the aerosols particles, which is explained more in detail in the following chapters.

Direct radiation is directional because it comes from a point source, the sun. The diffuse radiation comes from many different directions and involves the scattered light and the reflected radiation.

The scattering happens as a result of the activities of the aerosols. There are different types of scattering, in this thesis Rayleigh and Mie Scattering are described due to their importance in the circumsolar radiation.

Rayleigh Scattering concerns the scattering of light because of the molecules in the air and the tiny particles. As one can see in the figure 3, it strongly depends on the wavelength. Rayleigh Scattering occurs with particles about a tenth of the wavelength of the light; therefore the particles have to be of a very small size in order to scatter the wavelengths of the visible spectrum. Rayleigh Scattering causes the blue colour of the sky.

Mie Scattering occurs when the light and a large particle interact. The particle absorbs part of the light and the other part is reflected. Contrary to Rayleigh Scattering, Mie Scattering is not heavily dependent on the wavelengths. This type of scattering produces the colour of the clouds. The majority of the circumsolar radiation is produced as a result of Mie scattering. One can observe in the figure 4 how Mie and Rayleigh scattering interacts with the light. Mie scattering is dependent on the direction of the light, but Rayleigh not.
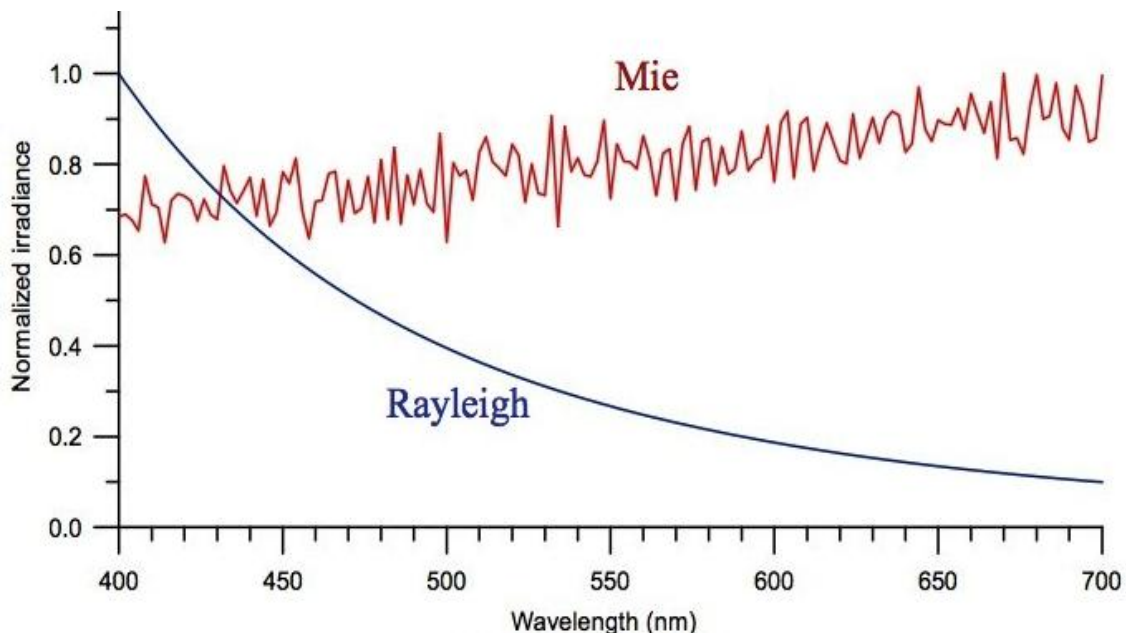
Figure 3: Wavelength dependence in Rayleigh and Mie scattering. /9/
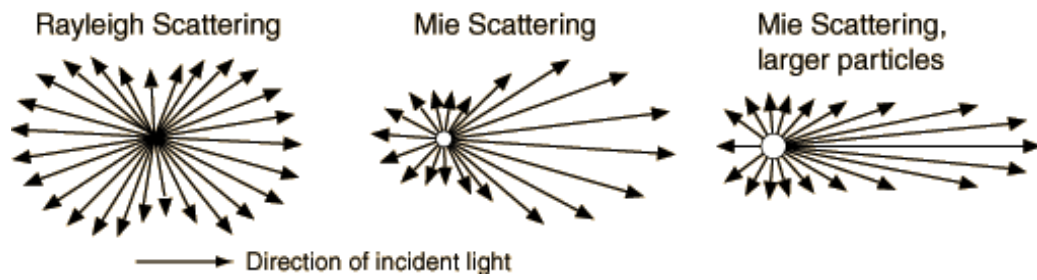
Figure 4: Scattering of the incident light. /10/

3. Circumsolar Radiation

3.1. Description

Circumsolar radiation refers to the radiation that appears to originate from the region around the geometric well-defined sun shape. When observing the sun from the ground, it is visible as the "solar aureole". The circumsolar radiation can easily be observed by blocking the solar disc and analyzing the light that flows around the covered sun shape. In figure 5, one can observe this aureole around the solar disc. The photo was used in this thesis in order to measure the circumsolar ratio (CSR) data.

Fi

Figure 5: Photograph of the sun and its "solar aureole", taken on 10.01.2012

Circumsolar radiation is caused by aerosol particles forward scattering light through small angles. These aerosol particles are present in the atmosphere and have dimensions equal to or larger than the light wavelengths.

The aerosols can cause for a significant part of the solar radiation to be diffused to angles of numerous degrees, but in these cases, the light is measured as diffuse radiation. If the

light is forward scattered into small angles, it is still registered as direct radiation. This is a consequence of the measurement method of the direct radiation, made with a pyrheliometer. Pyrheliometers have a typical field of view optical/visual range of 5 degrees to 6 degrees. The sun, viewed from the earth, has a diameter of 9.3 mrad, which is equivalent to 0.533 degrees /11/. The data registered as direct radiation by the pyrheliometer thus also includes a great quantity of the circumsolar radiation, overestimating the amount of energy that would be collected by a concentrating system. The circumsolar radiation reach the heliostats with a light angle deviation from the sun direction, then when the circumsolar radiation is reflected by the heliostats, part of it reach not the absorber.

3.2. Circumsolar ratio

The circumsolar ratio (CSR) is defined as the radiant flux contained within the circumsolar region of the sky Φcs and divided by the incident radiant flux from the direct beam and aureole Φi. /12/

$$CSR = \frac{\Phi\ cs}{\Phi\ i}$$

Equation 3: CSR equation

The direct beam radiation is the radiant flux collected exclusively from the solar disc. It is calculated with the following equation:

$$\Phi_{i,cs} = 2\pi \int_{0,\theta_\delta}^{\theta_\Delta} \phi(\theta) \sin(\theta) d\theta$$

Equation 4: direct beam radiation

With the same equation but with θ_Δ as the radiant displacement of the pyrheliometer, one can calculate the radiant flux contained in the circumsolar region.

3. 3 Previous studies

To date there are several studies concerning circumsolar radiation, the most important ones from the Lawrence Berkeley Laboratory (LBL) in Berkeley, United States, and the German

Analysis of aerosol particles for the determination of energy losses in solar power plants

Aerospace Centre (Deutsches Zentrum für Luft- und Raumfahrt, DLR) in Cologne, Germany.

The LBL collected data for about ten years from eleven different places across the United States. The locations have distinct atmospheric characteristics (for example humidity, altitude, climate, proximity to sources of large particles, etc.), and a wide range of data was obtained. About 200000 measurements were taken from the mid to late 1970s and in the early 1980s.

The measurements were all taken with the same telescopes, which measured a radial profile of the sun out to an angular displacement of 56 mrad. The telescope used as its basic optical element an off-axis mirror of 7.5 cm diameter and 1 m focal length. The telescopes functioned automatically and on its own for up to one week and collected one measurement every minute. A fused silica window protected the mirror from the environment. The mirror formed an image of the sun and the sky around it on a plate next to the telescope axis. A small hole in this plate, the detector aperture, defined the angular resolution (1/20 of the solar diameter), and the amount of light passing through the aperture into the detector assembly constituted the fundamental measurement. In the detector assembly the light was mechanically chopped, optically filtered, and focused onto a pyroelectric (thermal) detector. This type of detector was chosen for its uniform wavelength response in the 0.3 to 2.5 micrometer region, as well as its wide dynamic range.

The telescope scanned through a 6 degree arc with the sun at the center and measured the intensity of the solar and circumsolar radiation based on the angle. The instrument scanned in declination so that at sunrise and sunset it travelled nearly parallel to the horizon and at noon it moved in a vertical plane.

Each 6 degree scan required 1 minute of time. The intensity was registered every 1.5' of arc. Within 0.5 degrees on either side of the sun, an aperture of a size of 1.5' of arc was used, and outside this region the aperture was increased to 4.5' of arc. One set of measurements consisted in one scan at each of 10 filter positions: eight optical filters, one open (or clear) position, and one opaque position. The opaque position was used to measure the detector noise. The absolute determination of the normal incident flux (within 2.5 degrees of the sun's center) was provided by an active cavity radiometer. This device was self-calibrating and had an accuracy of 0.5%. The pyrheliometer was provided with a matched set of filters, which rotated synchronously to those on the scanning telescope. Thus the telescopes produced an absolute measurement of the normal incident flux, along with the

detailed solar profile in eight wavelength bands. Two pyranometers were used, one set up in the usual horizontal position and the other one tracking the sun.

The results show that there was a big variation of the CSR data depending on the place where the measurements were taken. These locations were very far apart and they had very different conditions, but these conditions were not considered in order to compare the obtained CSR data. In the figure 6, one can observe the fluctuations in the measurements. /12/

The DLR have designed and created a digital sunshape camera using an optical telescope together with a 12-bit digital resolution CCD camera. Using this camera, 2300 solar profiles were acquired from three sites across Europe: the DLR site in Cologne (Germany), the PSA in Almería (Spain) and the CNRS Solar Furnace in Odeillo (France). These profiles were grouped and averaged according to each sunshape's CSR, using a method similar to the one applied to the RDB in this thesis, however, accepting larger ranges of CSRs for each sunshape bin.

The optical system of the DLR's telescope includes a band pass, neutral density filter. This is used together with the CCD camera in order to improve the spectral response of the CCD's silicon wafer.

The solid angle subtended by each element in the CCD camera used by the DLR telescope is 0.065 millisteradians (msr). The equivalent figure for the LBL's telescopes was 0.44 msr, which demonstrates the lower spatial resolution of the LBL data. This improvement by the DLR provides both a greater number of data points to be recorded across the transition between the solar disk and the circumsolar region, and higher quality data for each image point. Also, the time required for the DLR to acquire an image with the CCD camera was virtually instantaneous, compared to scans from LBL lasting 1 min. The shorter time span provides a higher probability of acquiring self-consistent profiles. /11/

In the figure 6, one can observe and compare measurements taken by the DLR and by the LBL. Each colour represents a measurement of the brightness of the sun sphere considering its angular displacement. One can observe that these measurements had different results. /12/
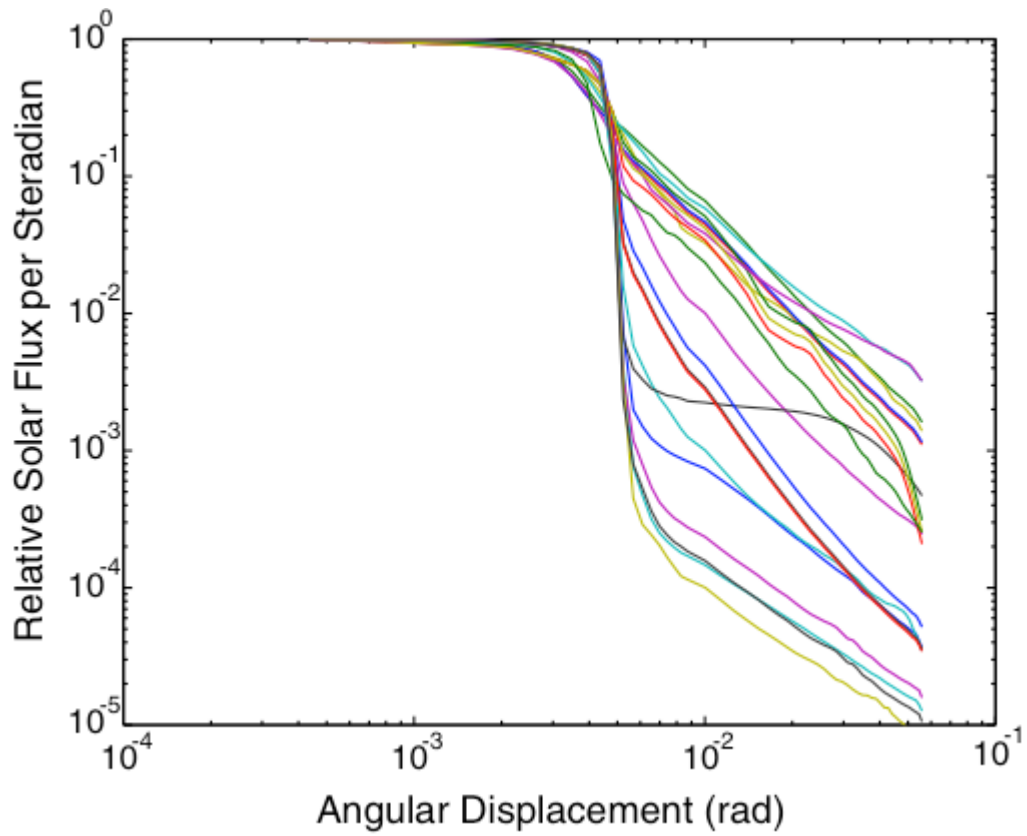
Figure 6: results of the measurements made by the LBL and the DLR /12/

4. Aerosols

4.1. Description

Technically, an aerosol is a suspension of fine solid particles or liquid droplets in a gas. The sizes of these particles can vary from 0,002 mm to 100 mm. The smallest ones are molecules in the air, which can remain in the air or a gas for weeks, but the larger they are, less time they can remain suspended. Particles with a size over 10 mm cannot be suspended more than a few hours due to the gravity effect. The majority of the small particles disappear because of precipitations.

Particulate matter (PM) is the term used for liquid droplets or solid particles suspended in a gas. There are two main groups to distinguish the PM: coarse and fine particles. Coarse particles have an aerodynamic diameter larger than 2.5 mm, and fine particles one smaller than 2.5 mm. The aerodynamic diameter of an irregular shaped particle is the diameter of the spherical particle with a density of 1000 kg/m³ that has the same settling velocity as the irregular particle. In this thesis, the sizes which will be used are PM 1, PM 2.5, PM 4, PM 10 and PM total. They refer to particles with an aerodynamic diameter smaller than 1, 2.5, 4, 10 mm and the total amount of the particles suspended in the air.

Aerosols can also be measured by weight per volume. The total amount of the aerosols in the air varies between 1 mg/m³ (as can be found at the polar cap or in the free troposphere above the oceans) and 1000 mg/m³ (in a wildfire or in desert sandstorms).

4.2. Composition:

The aerosols can also be classified in different groups according to the substances they are made up of, such as sulphates, organic carbon, black carbon, nitrates, mineral dust, and sea salt. In reality, however, the particles are usually more complex, consisting of more than only one substance, which makes it difficult to group them according to their composition. /13/

4.3. Origin

The majority of the aerosols (about 90 percent) is of natural origin, like volcanic ash, the smoke of wildfires or the mineral dust in deserts. The remaining 10 percent has anthropo-

genic origin, mainly from the burning of fuel. While these aerosols appear much less, they can be found at very high concentrations in the air in big cities. The most common aerosols are:

4.3.1. Of natural origin:

Soil dust: it comes from elements which occur in the composition of soils. Due to the effect of wind this mineral dust is eroded from the crust. These aerosols consist mainly in oxides (SiO_2, Al_2O_3, FeO, Fe_2O_3, CaO, etc.) and carbonates (CaCO·, $MgCO_3$) that which appear in the earth's crust. The annual mineral dust emissions are estimated between 1000 and 5000 millions tonnes per year, the majority of which comes from the deserts. The main sources are the Sahara and the Gobi desert. The figure 7 shows the dust concentration on a global scale. Although the source of these aerosols is considered natural, it is estimated that around 30 percent of the mineral dust is produced due to the human action, by activities that increase the desertification.
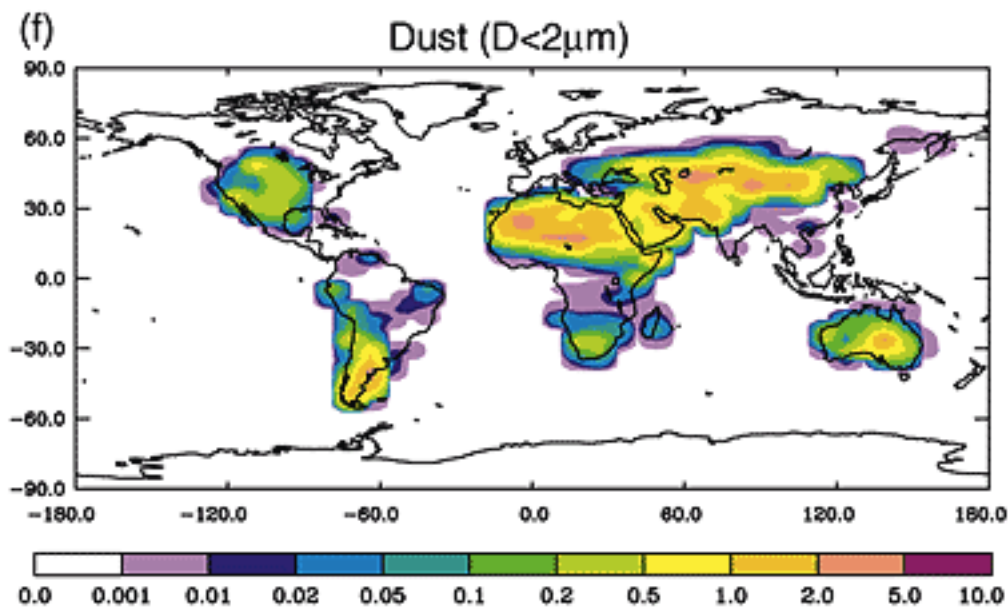
Figure 7: dust concentration in the world /13/

Sea salt: when a wave in the sea breaks, because of the wind, some amount of water gets into the air in the form of small particles. The composition of these particles is the same as that of seawater: substances such as water, sodium chloride and magnesium and sulphate salts. This type of aerosol scatters the sun light and forms clouds. The sea salt particles are quite large, so they cannot travel very far away and usually fall down over the sea.

Primary biogenic aerosols: they are composed of plant debris, humic matter and microbial particles. They are present in areas with intense vegetation.

Volcanoes: they eject huge columns of ash, sulphur and other gases to the air. The sulphate aerosol particles, which are in the upper troposphere, contribute to the formation of clouds. This contributes to the cooling effect called the "indirect aerosol effect", further explained at the end of this chapter. The figure 8 shows measurements taken by the Mauna Loa Observatory, where the solar radiation which has been transmitted over the last fifty years is shown. The influence of the volcanic eruptions on the percentage of transmitted solar radiation is clearly visible.
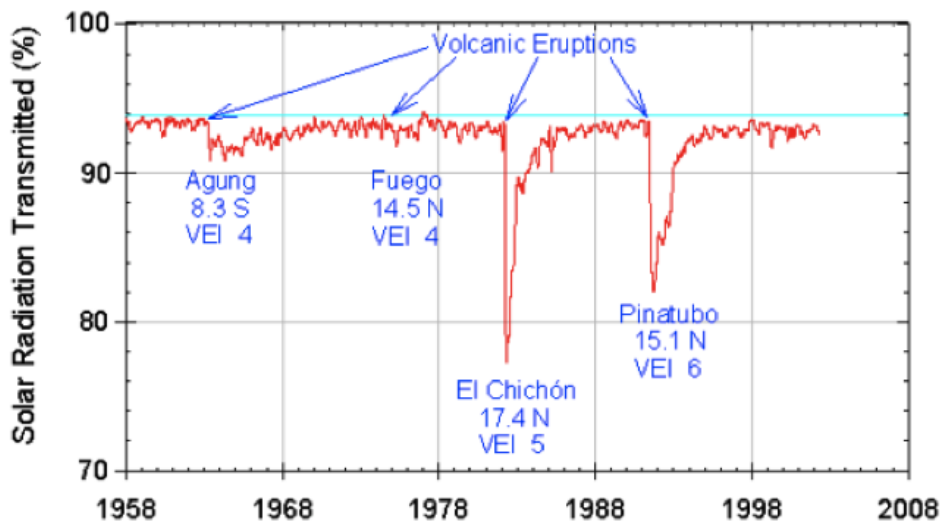
Figure 8: Solar Radiation Transmitted by Mauna Loa Observatory /14/

4.3.2. Of anthropogenic origin:

Sulphates and nitrates: these are secondary particles which are produced from the reaction of primary gases (sulphur oxide and nitrate oxide NO_x) in acids (gaseous nitric acid and liquid sulphuric acid). They can be formed with or without ammoniac. The origins might vary: either of natural origin (volcanoes or sea plankton) or of anthropogenic origin (fuel combustion). Both types cause heavy light scattering.

Organic and black carbon: Organic elements represent the largest single component of biomass burning aerosols. Organic aerosols are important constituents off the highest part

of the troposphere. They are water-soluble and contribute to the nucleation of cloud droplets. The black carbon has a light absorbing character.

Industrial dust: coal combustion, traffic, construction, waste incineration and other industrial activities produce primary aerosol particles. In the developed countries, the amount of these particulates has decreased in the last years, but it is increasing in the newly industrialising countries. While this signifies a big environmental problem, it doesn't have great consequences on the light scattering due to the large size of the particulates.

4.4. The influence of the aerosols on the solar light scattering

In this thesis the influence of the aerosols on the solar radiation is studied, so it is necessary to explain how these particles affect the incoming solar radiation. Some first studies have been made about the capacity of the aerosols to modify the radiation balance. These studies were done with anthropogenic particles, like sulphate aerosol (SO^2) or products from the burning of biomass. Scientists as Charlson Kiehl and Brieglev estimate that these aerosols could backscatter a quantity from -1 up to -2W/m^2 to space. The aerosols can affect the climate in two different ways: directly and indirectly.

4.4.1. Direct effect

Aerosol particles in the atmosphere reflect or scatter solar radiation depending on their size. As explained in Chapter 2, the solar radiation spectrum has a wide range of wavelengths, and the aerosols particles interact with those of a similar size. In the figure 9, four different examples of the interaction of particles and solar light are given. The first one shows the effect of a very small particle: there is not a big influence of the particle on the wave. When the size of the particle is very large (>10 mm), there is also no scatter. In the second example, large particles (over 2 mm) were used, and they caused Mie scattering, where the light is scattered at a small extent. The third one shows how Rayleigh and Mie scattering occur. The particles interact with wavelengths of a similar size, in this case with the particles in the range of the visible light, which contains the majority of the solar energy. The wave is reflected by the particle and it is scattered, part of it out to space. Furtheron, there are also particles that absorb light. They are coloured, and the radiation causes them to heat up. The large particles previously mentioned can also be coloured and absorb the sunlight.
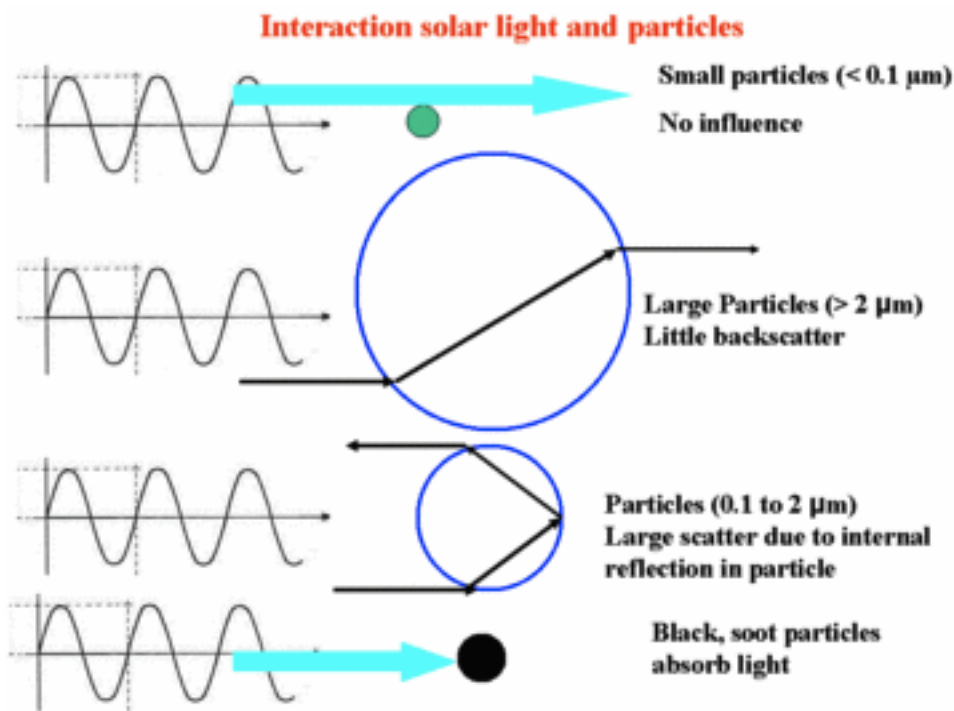
Figure 9: Interaction of solar light and particles /15/

4.4.2. Indirect effect

Cloud formation is dependent on aerosols. If there are not aerosols, super saturation (relative humidity) can be seen without droplet formation. Cloud droplets need aerosols to be condensed. If not much particles are present (less than 200 per m³) the droplets will be large, but if there are a lot of aerosols present, smaller droplets will be formed.

Clouds with big droplets reflect less light compared to clouds with small droplets. The high cirrus clouds, which have large droplets, do not reflect much solar light but they reflect the long wave infrared radiation better. So this way aerosols have an indirect effect on the climate. This will be explained more in detail in Chapter 5.

The figure 10 shows the relation between the number of aerosols particles and the number of droplets. As can be seen, the relation is not lineal, as of 1000 particles per m³ the effect stops increasing and remains at a steady constant.
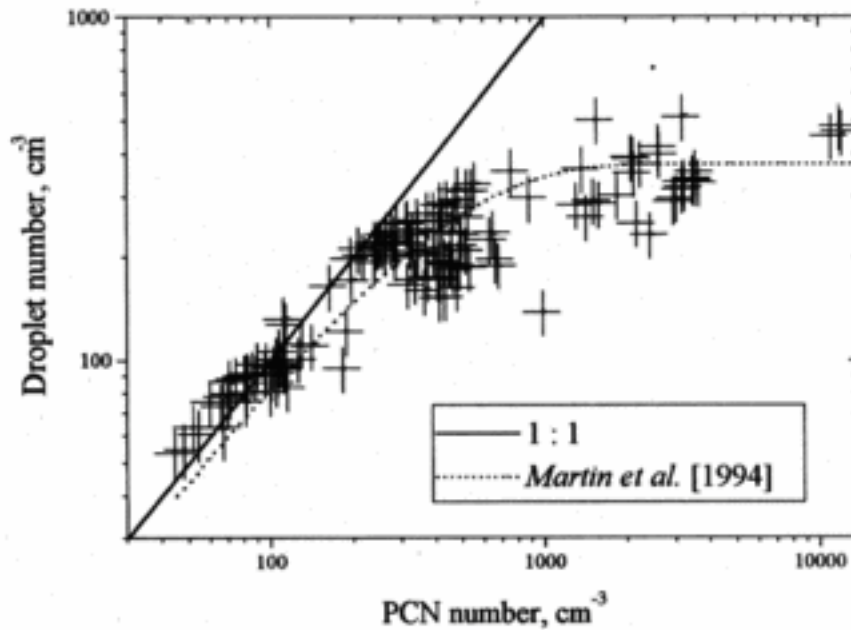
Figure 10. Number of droplets per volume in relation to the number of particles per volume. /15/

4.4.3. Impact of direct and indirect aerosol effect:

As estimated by the Intergovernmental Panel on Climate Change (IPCC), aerosols represent about 30% of the driving power of greenhouse gases.

According to the IPCC, the warming effect of the greenhouse gases is 2.5 W/m², while the cooling effect of aerosols would be 0.7 W/m². After adding them, the net result is thus a warming effect of 1.8 W/m².

5. Clouds

5.1. Description

The clouds have a very important impact on the scattering of the solar radiation. In this chapter, it is going to be exposed how solar radiation and the different types of clouds interact.

A cloud is visible mass made up of liquid water droplets or ice crystals and other chemicals suspended in the atmosphere. Clouds are also considered as aerosols. The size of the diameter of these droplets varies between 5 and 100 µm. In order for them to turn into a raindrop, their diameter needs to be bigger than 1 mm. The concentration of the droplets in a cloud varies between 25000 and 1 million droplets per air litre.

Clouds significantly influence the climate and the solar radiation, both the incoming radiation from the sun and the outgoing radiation from the earth. The thick clouds, which are situated at a lower height, reflect solar radiation, thus cooling the surface of the Earth. The thin clouds, which are situated at a higher level, primarily transmit incoming solar radiation, but they also reflect the outgoing infrared radiation emitted by the surface of the Earth, which causes a warming of the Earth's surface. /16/

5.2. Reflection caused by the clouds

Every surface reflects the light, and the clouds are not an exception. This reflection is called albedo. A high albedo means that a large portion of the sun's energy is reflected; snow, deserts or clouds are examples of this. Then there are also low albedos, which only reflect a small part of the radiation and absorb the rest; oceans or rain forest surfaces have low albedos. About 30 percent of the incoming solar energy to the Earth is reflected back to space, mainly due to the clouds. In the figure 11 appears the different albedos for different surfaces and clouds.
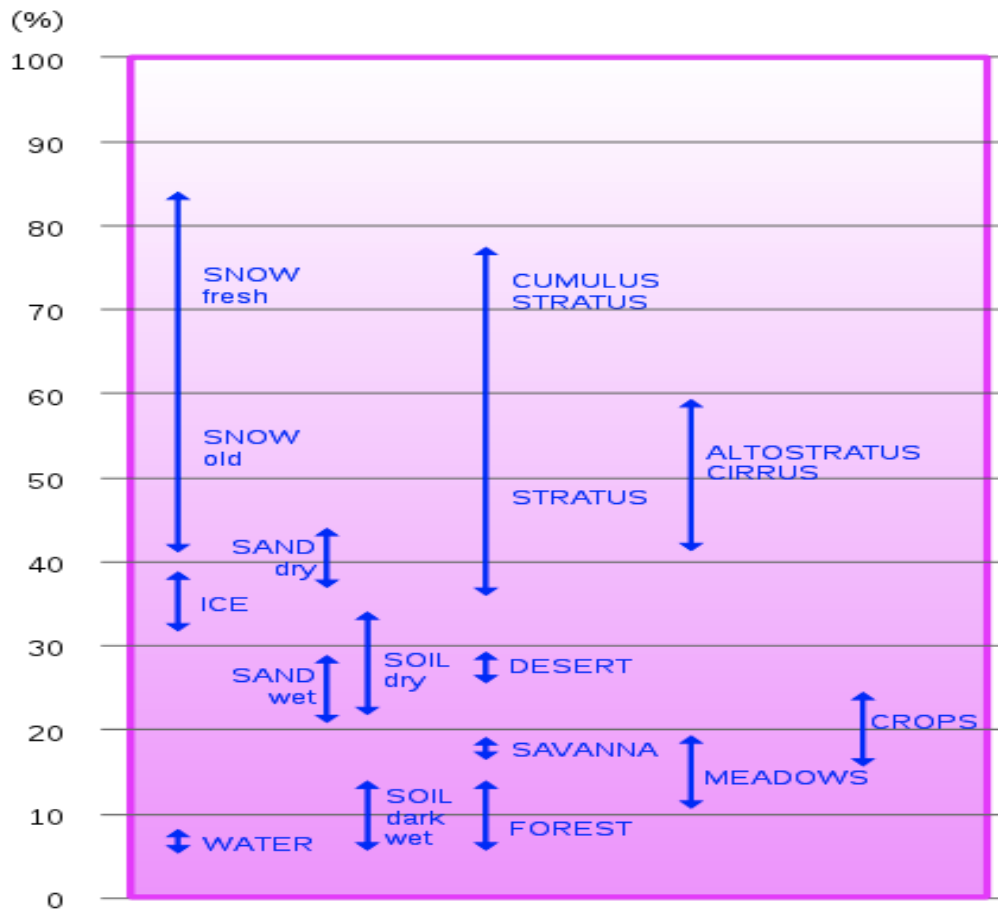
Figure 11: Albedos for different surfaces. /17/

Most of the incoming energy from the sun is transmitted in short wavelengths. The image below shows what happens when a thick cloud and short wavelengths interact. As one can see the majority of the wavelengths are reflected by the cloud, which illustrates a high albedo.
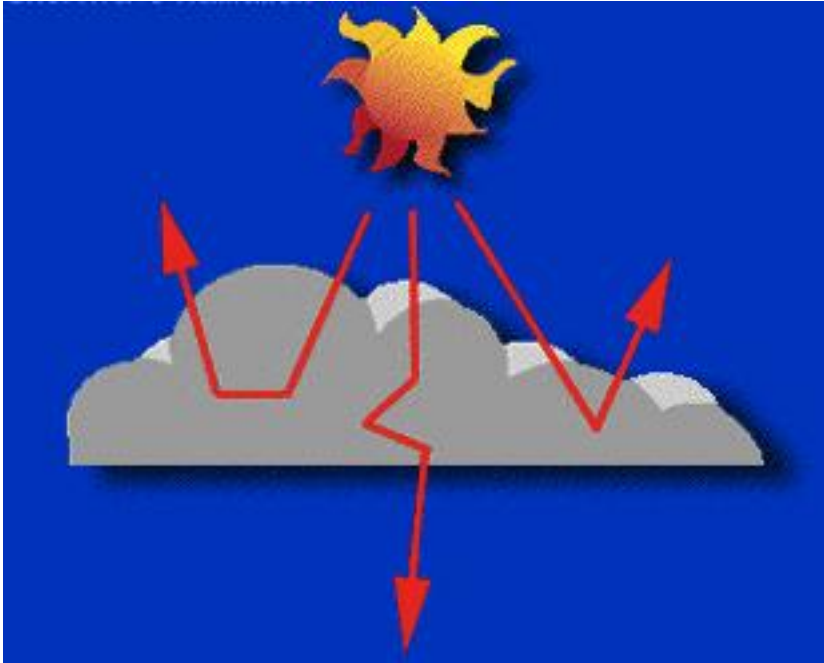
Figure 12: Shortwave radiation reflected by a thick cloud. /18/

The clouds also backscatter the electromagnetic radiation that is emitted by the Earth. The Earth reflects a big part of the radiation from the sun, which was explained before with the albedo, but also the radiation emitted by the Earth. Every object with a temperature higher than the zero absolute (-273K), radiates energy. Then the energy, which was absorbed before, is going to be reflected later. The wavelengths of this radiation are longer than the solar radiation waves, and they are not visible to the human eye. A portion of this radiation can also be reflected by the clouds and returned back to the earth, which produces a heating of the Earth's surface. This process is called "cloud greenhouse forcing". It is a phenomenon common with thin clouds, caused by their interaction with long wavelengths. In the figure 13 one can see how a cloud interacts with the long wave radiation emitted by the earth.
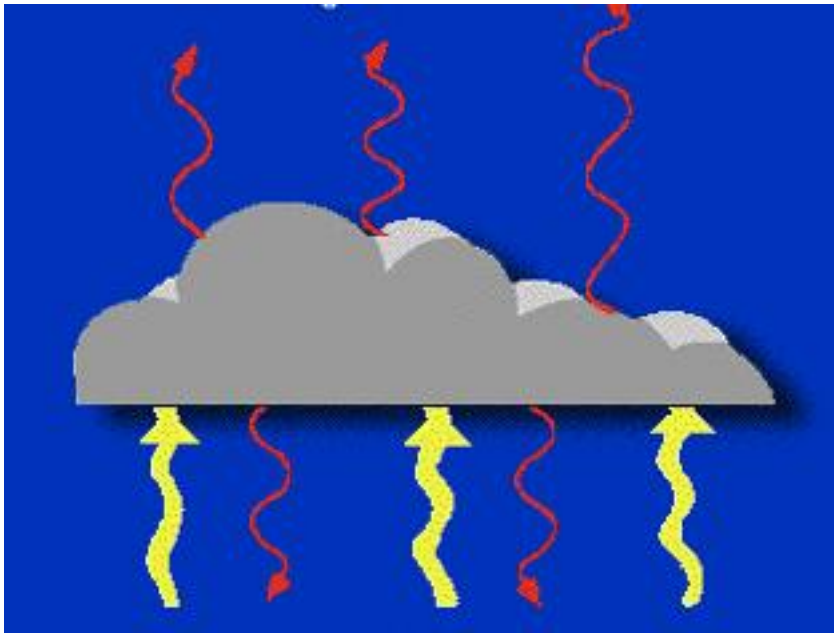
Figure 13: reflection of the electromagnetic radiation emitted from the Earth. /18/

5.3. Types of clouds:

There are many types of clouds; they are first of all divided into groups according to their expansion form: stratiform or vertical; then they can be classified in three groups according to their height: high, medium and low clouds. One can further differentiate different kinds of clouds depending on their composition and form. This thesis is going to be focused on the stratiform clouds.
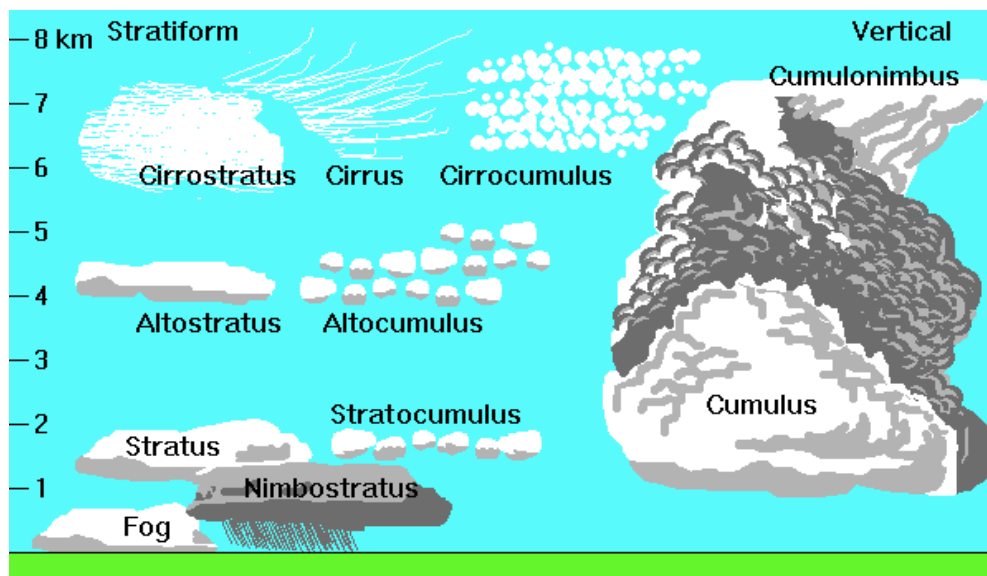
Figure 14: Types of clouds

5.3.1. High clouds:

The high clouds are located between 5000 and 12000 meters in regions with a temperate climate. They are usually thin and of a white colour, which can, however, change during the sunset or the sunrise.

As these clouds are thin, the backscattering produced by them is not too high; the direct radiation can thus pass through these clouds.

High clouds are divided into three groups: cirrus, cirrostratus and cirrocumulus. In the figure 15, a cirrostratus is shown. As can be seen, the sun can be observed through the cirrus cloud. /19/

Figure 15: Cirrostratus cloud

High clouds are normally wispy and have a large droplet size. Since they do not backscatter much shortwave radiation, they do not have a high albedo. But it is different with the longwave radiation. The cirrus clouds can absorb the Earth's infrared radiation and then emit long wavelength radiation back to the earth or out to the space. In the figure 16 one can observe the short wavelength radiation (red lines) and the long wavelength radiation (yellow lines). The short wavelength radiation is hardly scattered by high clouds due to its large droplet size. This scattered radiation will not be direct radiation if it reaches the earth surface. It will be diffuse radiation, which could be part of the circumsolar radiation studied in this thesis. The long wavelength radiation is backscattered by the cloud and causes the "cloud greenhouse forcing". The high clouds are the most important ones for the purposes of this thesis.
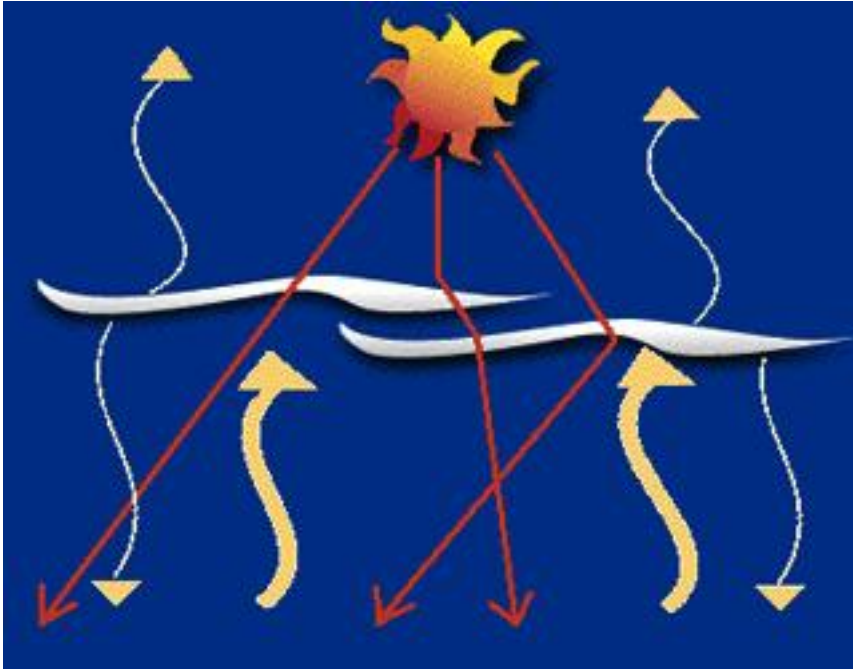
Figure 16: scattering by high clouds /18/

5.3.2. Middle clouds:

They are located between 2000 and 7000 meters. These clouds are made of water, and when it is freezing, ice droplets. Their colours are white, grey or both. Normally they are in groups and they do not cover the whole sky. The middle clouds reflect part of the sun light and the rest is normally scattered, so they produce diffuse radiation.

Figure 17: Altocumulus cloud

5.3.3. Low clouds:

There are many types of low clouds, but this thesis is only focused on stratocumulus clouds. The stratocumulus clouds are situated under 2000 m from the earth surface. And in contrast to the high clouds, they cool the atmosphere due to their high albedo. They are much thicker and have a smaller droplet size than the high clouds and, as a result, the sun waves cannot pass through them and are backscattered. These clouds also emit longwave radiation, to the space and towards to the earth. But as they are not very high, their temperature is similar as in the earth surface, so they radiate almost the same intensity as the earth surface. The figure bellow shows a scheme with the different radiations and these clouds.
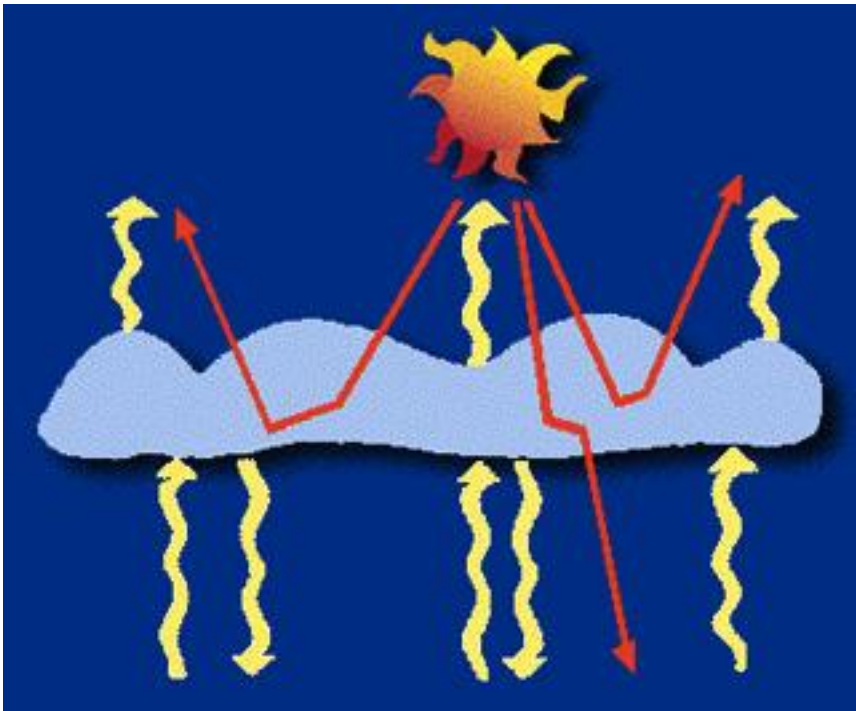
Figure 18: Low clouds and solar radiation /18/

6. Ceilometer: CHM 15K

For the measurements of the height of the aerosol particles and the clouds, as well as their concentrations, a CHM15k ceilometer was used. With this machine it is possible to make measurements of particles in a height of up to 15 km.

The machine used in the work for this thesis is located on the roof of the Naturwissen-schaft-building, on the FH Aachen campus, in the city of Jülich.

The machine works based on the LIDAR-method (Light Detection And Ranging), an optical sensing technology that can measure the distance, and other properties of objects in the atmosphere using pulses from a laser. The method is similar to that of radar, which determines how far the target is away, depending on the delay between the emitted and the reflected signal. But in this case it works with light, not with radio waves. The LIDAR technology is mostly used to measure geographical characteristics and to develop maps, but it has more applications.

LIDAR uses wavelengths between 10 micrometers and 250 nanometres. As a result, the spectrum reaches from ultraviolet to visible and infrared light. As discussed in previous chapters, the laser works in a range similar to that of the solar spectrum, so it is going to be useful to measure particles in the atmosphere, which influence the sunlight. These are clouds, raindrops, aerosols and even molecules. The laser pulses interact with the different particles via scattering. The most usual scattering mechanism is Mie scattering.

Figure 19 gives a sketch of how the LIDAR technique works:
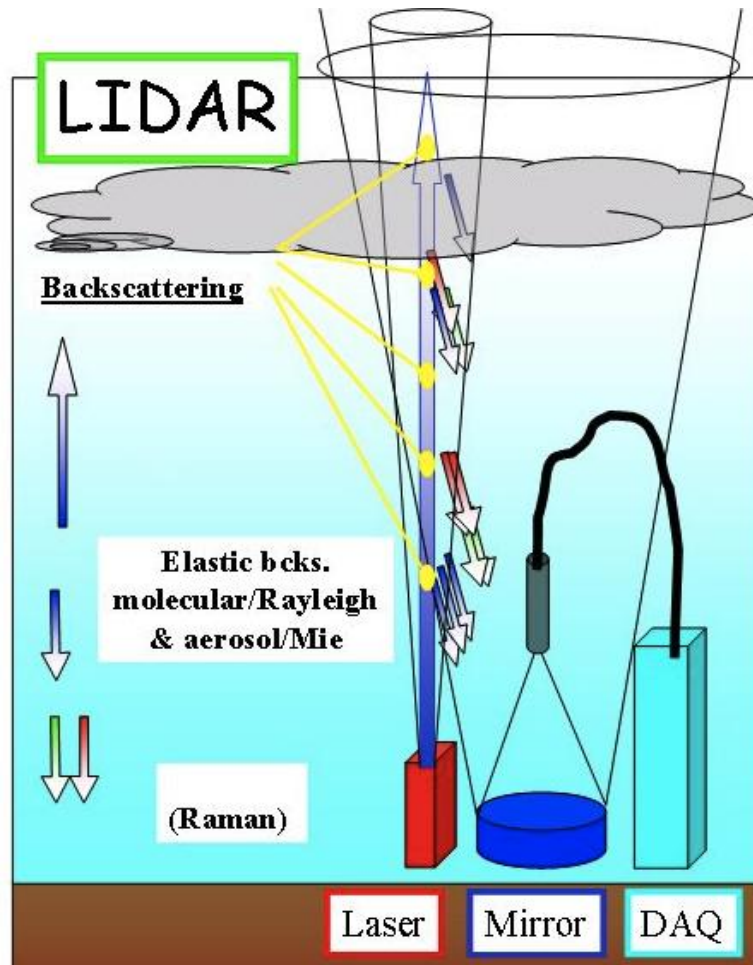
Figure 19: Operating principle of LIDAR. /20/

In the ceilometer, a laser points vertical towards the sky and there is a receiver next to it. The duration of the laser pulse is several nanoseconds, and it is directed vertically through the atmosphere. When the beam crosses through the atmosphere, a fraction of it is scattered by particles in the air, normally with sizes similar to those of the wavelengths of the laser. This form of scattering is called Mie scattering. A small part of the scattered light will return to the LIDAR receiver. The time t between the emitted laser signal and the signal measured in the receiver will give the distance of the particles, which were involved in the scattering process. The distance R can be calculated with the following equation:

$$R = \frac{t \cdot c_{air}}{2}$$

Equation 6: Distance /21/

Where c_{air} is the speed of light in air.

Analysis of aerosol particles for the determination of energy losses in solar power plants

To measure the power of the light scattered back and received by the LIDAR detector, the following equation is used:

$$P(R) = K \cdot G(R) \cdot \beta(R) \cdot T(R)$$

Equation 7: Power of the light received by the LIDAR /21/

It consists of four different parts, which are described below:

K is an experimental regulation parameter, which is calculated using the following formula:

$$K = P_0 \cdot \frac{C\tau}{2} \cdot A \cdot \eta$$

Equation 8: LIDAR experimental regulation parameter /21/

Where P_0 is the average power of a single laser pulse, c is the speed of light in air, τ is the time duration of a pulse, A is the area of the receiver and η is the total system efficiency. K is a system-specific parameter and constant in the system.

G (R) is a geometry factor. It is calculated with the following formula:

$$G(R) = \frac{O(R)}{R^2}$$

Equation 9: geometry factor /21/

Where O (R) is the overlap function of the laser beam and the field of view of the receiver. And R is the distance of the particles as mentioned before.

The parameter β is the backscattering coefficient, which determines the power of the signal received on the ground. The equation is an addition of the intensity due to both Rayleigh scattering and the Mie scattering.

$$\beta(R, \lambda) = \beta_{mol}(R, \lambda) + \beta_{aer}(R, \lambda)$$

Equation 10 backscattering coefficient /21/

T is the transmission term. It describes the quantity of light lost in the atmosphere before being scattered. With the Lambert-Beer-Bouguer law, these losses can be determined:

Analysis of aerosol particles for the determination of energy losses in solar power plants

$$T(R, \lambda) = exp\left[-2 \int_0^R \alpha(r, \lambda)dr\right]$$

Equation 11 /21/

Where $\alpha(R,\lambda)$ gives a ratio of how much intensity is lost after the light crosses through a distance R in a gas. The integral describes the path of the light from the laser and back to the receiver.

The dependence of $\beta(R,\lambda)$ and $\alpha(R,\lambda)$ of the wavelength of the laser light is determined by the size, refractive index and form of the scattering particles.

In the work for this thesis a CHM 15k ceilometer from the German company Jenoptik was used, as shown in figure 20. Furthermore, the technical specifications of the ceilometer are given in table 1.

Figure 20: CHM 15K used in this thesis.

Analysis of aerosol particles for the determination of energy losses in solar power plants

MEASURING PARAMETERS	
Measuring principle	Optical (LIDAR)
Measuring range	15- 15000m
Accuracy	±5m
Resolution of backscatter data	Standard: 5m Optional: 15m
Hardware resolution	200 Mhz (sampling rate)
Time to measure	5s to 60min (programmable)
Targets	Aerosols, clouds
Quantities to be measured	- Cloud base (max. 5 layers, preset: 3 layers) - Cloud amount - Penetration depth - Vertical visibility - Height of mixing layer
Light source	Nd:YAGsolid - statelaser, wavelength 1064 nm
INTERFACES AND SOFTWARE FOR DATA OUTPUT AND DEVICE CONFIGURATION	
Standard interface	RS485
Optional interfaces	RS232, RS422, LAN, CIBUS
Communication	Measured data and settings are transmitted in data telegrams. Easy device configuration and firmware upgrades with JO-Data Client software.
Optional software	JO-Visual Software for convenient visualizing measured results
ELECTRICAL PARAMETERS	
Power supply	230 / 110 V(AC), ±10 %
Power consumption	250 W (standard) 800 W (in maximum heating mode)
OPERATING SAFETY	
Environmental compliance	ISO 10109-11
Laser protection class	1M according to DIN EN 60825-1
Internal protection class	IP 65
EMC	Class B, DIN EN 61326-1
Electrical safety	DIN EN 61010-1

Certifications	CE
OPERATING CONDITIONS	
Temperature	-40 °C ... +55 °C
Relative humidity	0 % ... 100 %

Table 1: technical specifications of CHM 15K /22/

7. Aerosol spectrometer: FIDAS ® 200:

For taking measurements of the aerosols on the ground level it has been used a light scattering photometer, the Fidas ® 200.

The machine used in this thesis is located on the roof of the Naturwissenschaft building, in the FH Aachen campus in the city of Jülich.

The Fidas® continuous ambient air quality monitoring service provides continuous and simultaneous PM1, PM2.5, PM4, PM10, TSP (total suspended matter) and the particle number concentration.

The system uses the approved measurement technology of optical light scattering and is equipped with a LED light source with stable output and long lifetime.

The machine operates with an aerosol flow of 5l/min and is equipped with a Sigma-2 sampling head according to VDI 2119-4, which allows a representative measurement even at strong winds. Fidas ® 200 provides an Intelligent Aerosol Drying System (IADS) as well as sensors for the measurement of ambient temperature, air pressure and relative humidity.

Principle of operation:

In the following scheme it can be seen the different parts of the Fidas ® 200, then is going to be explained its principle of operation.
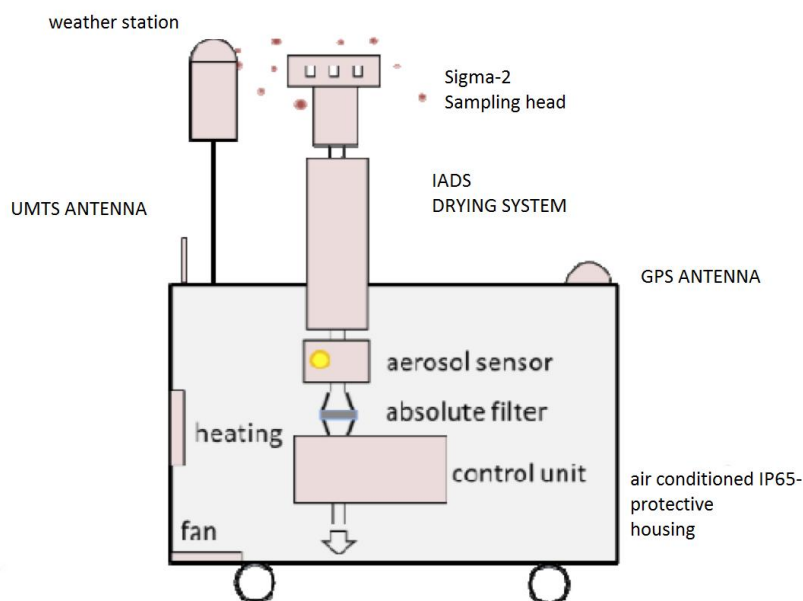

Figure 21: principle of operation of the Fidas 200.

The air get into the sigma-2 sampling head, then the IADS avoids, that the particle size measurement is effected because of moisture, by using a dynamically regulated drying system in regards to relative humidity and ambient temperature.

The aerosol sensor is an optical aerosol spectrometer that determines the particle size and number by a scattered light analysis after Mie scattering. The particle move separately through an optically differentiated measurement volume, homogeneously illuminated with white light. Each particle generates a scattered light impulse, detected at an angle of 85° to 95°. The number concentration is deducted from the number of scattered light impulses. The intensity of the scattered light is a measure for the particle size diameter.

The lower detection limit was reduced to 180 nm by using optimised optics, higher light density and improved signal analysis (logarithmic analog digital converter). Therefore smaller particles, measured roadside in high concentration, are better accounted for.

The better the classification precision and the resolution capacity, the much preciser is the definition of the particle size distribution.

Using a white light source, a precise calibration curve without ambiguity can be achieved, resulting in an extremely high size resolution. The patented T-aperture leads to an accurately defined optical measurement volume and permits a particle measurement without border-zone-errors and therefore a precise size measurement. The new and quick digitalised signal electronic analysis allows the identification and correction of coincidence.

For the conversion of the measured indicators into mass or mass fractions, the high resolution particle size distribution will be multiplied in each value with a correlation factor, representing that the aerosol particulate is build up from different sources (e.g. combustion aerosols, tire abrasion, pollen) according to its particle size. A mass fraction is achieved by applying an additional separation curve (e. g. DIN EN 481) to the determined particle size distribution.

Downstream to the optical sensor there is a filter holder for an optional gravimetric validation of measured data. /23/

In the following pictures one can observe the machine Fidas ® 200, and bellow there is a table with its technical parameters.

Figures 22 and 23: Fidas ® 200

Measuring principle	Optical light scattering
Reported Data (simultaneous)	PM1, PM2,5, PM4, PM10, TSP, number
Size channels (optional)	64
Measurement range (particle size)	0,18 – 18 μm
Measurement range (number)	1 – 20000 particle/cm3
Measurement range (mass)	0 – 1500 μg/m3
Time resolution	1 s – 24 h
Aerosol flow	5 l/min (0,3 m3/h)
Working temperature	-30 to +35°C
Power supply	115/230 V; 50/60 Hz
Power consumption	140 W
Dimensions	18.5x45x32cm
Weight	9.3 kg
Interface	Touch display 800 x 480 pixels
Data logger	4 GB Compact Flash
Network	LAN, WiFi

Table 2: technical specifications of Fidas 200 /23/

8. WEATHER STATION:

The Solar-Institut Jülich, where the measurements for this thesis were done, also features a weather station. This station was used to determine the following meteorological parameters: temperature (ºC), relative humidity (%), wind speed (m/s), wind direction (º), air pressure (hPa), precipitations (mm) and the global direct and indirect solar radiation per area (W/m2).

The weather station saves all this data on a hard drive every minute for the last five years.

8.1. Instruments:

The weather station is divided into two components: a weather mast and a solar tracker.

8.1.1 Weather mast:

The weather mast is situated about one hundred meters east of the roof where the other measurements are taken. The weather mast itself measures the air temperature, the relative humidity, the wind speed, wind direction, air pressure, precipitations and solar global radiation.

Figure 24: Weather mast located in Jülich

8.1.2 Solar-Tracker:

The Solar-Tracker is situated on the roof of the Naturwissenschaft-building, which is close to the ceilometer and the aerosol spectrometer, but four meters higher. It measures the direct and diffuse radiation, while tracking the sun throughout the day. A pyrheliometer is used to measure the direct radiation and a pyranometer to measure the diffuse radiation.

Figure 25: Solar tracker

8.2 Measurements of the solar radiation:

8.2.1 Global and diffuse radiation:

The global radiation is the sum of the direct radiation and the diffuse radiation, but not the reflected. It is measured with a device called pyranometer. The pyranometer is a type of actinometer, which measures broadband solar irradiance. The sensor has a black coating. The heating of this sensor is proportional to the incident radiation, which can be determined from the temperature difference to the environment. The pyranometer receives light irradiance from a field of view of 180 degrees.

The diffuse radiation is the global radiation minus the direct radiation. A pyranometer can be used to measure diffuse radiation too, but it is necessary to eliminate the direct radiation. To solve this problem, the pyranometer is joined with the solar tracker and an opaque body, that blocks out the direct solar light coming towards the pyranometer. The figure 26 shows a pyranomometer and the figure 27 give an idea about how is measured the direct and indirect radiation.
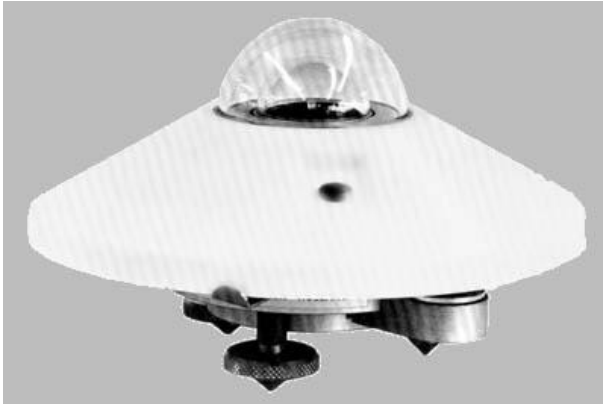
Figure 26: Pyranometer /1/
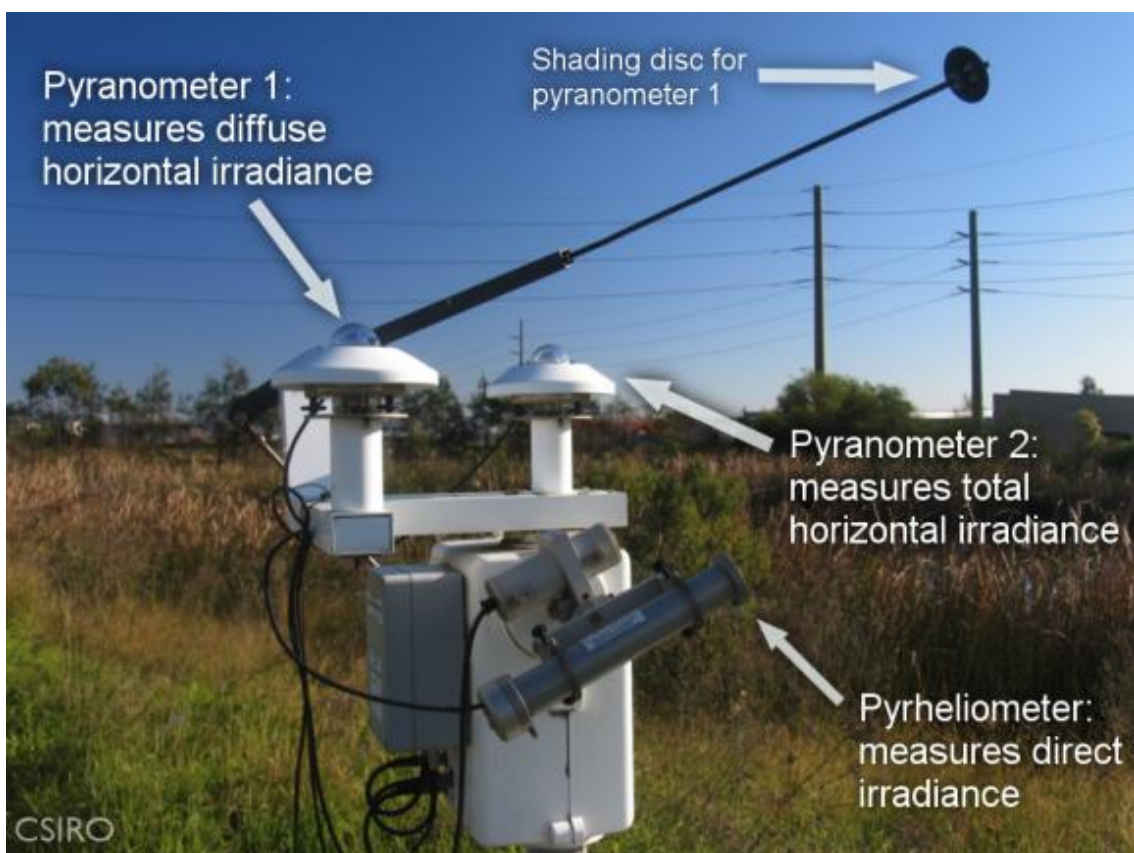
Figure 27: scheme of a solar tracker

8.2.2 Direct Radiation:

For the measurements of the direct radiation, a pyrheliometer is used. In order for it to work correctly, it must be connected to a solar tracker. To receive the whole incident flux of light, the pyrheliometer must be aligned with the sun, therefore it must follow the suns movements. The pyrheliometer works in a similar way as the pynamomter, but its sensor is

Analysis of aerosol particles for the determination of energy losses in solar power plants

at the end of a 30 cm tube, so that it only captures the direct radiation. In the figure 28 the pyrheliometer is shown.

Figure 28: Pyrheliometer

8.3 Other measurements:

8.3.1 Measurements of the air temperature:

A PT100 platinum resistance thermometer was used to measure the air temperature.

8.3.2 Measurements of the relative humidity:

A CPC 2 humidity sensor by the company " GalltecMela" was used to measure the relative humidity.

Figure 29: Relative humidity sensor (left) and temperature sensor (right) /1/

8.3.3 Measurements of the air pressure:

The sensor 144SC-Baro was used to measure the barometric pressure. It is manufactured by the company "Forschungstechnik und Computersysteme GmbH".

8.3.4 Measurements of the wind speed and direction:

Both of these measurements were taken with the Ultrasonic Anemometer 2D produced by the company "ThiesClima".

Figure 30: Anemometer /1/

8.3.5 Measurements of the precipitation:

The amount of rain was measured with a rain gauge; the model 7041.0000 from the company "Theodor Fiedrichs GmbH & Co." was used.

Figure 31: rain gauge /1/

9. Camera system

The following chapter is going to explain, how the CCD camera and the telephoto lens work. In addition to the principles of operation, the technical parameters of the devices will be presented and possible distortions that can occur in the photos will be discussed in detail.

9.1 Telephoto lens:

A telephoto lens is a system with a longer focal length and a smaller vision angle, than normal lenses. It magnifies the object several times and is used for taking pictures over long distances.

For taking pictures of the sun the telephoto is useful for two reasons:

The telephoto lens magnifies the object that is photographed, which allows analyzing the pictures in greater detail.

The telephoto lens allows concentrating the object in an image selection, therefore only the sun will appear in the pictures taken for the measurements.

The telephoto lens used for the work of this thesis was the WalimexPro 500mm/5.6 with manual focusing. The technical specifications of the telephoto lens are given in the chart below:

Focal length	500 mm
Aperture	F 5.6
Field of view	5.2°
Filter diameter	86 mm
Closest focusing distance	20 m
Lenses	3 Elements in 3 groups
Size	Approx. $\varnothing$90 * 412.5 mm

Table 3: technical specifications of the telephoto lens /23/

The depth of field depends on the aperture, focal length and shooting distance. A bigger focal length leads to a smaller depth of field. This means that a smaller distance range is in

focus. This can be a problem when taking pictures of the sun, because the circumsolar radiation and sun itself are not at the same distance from the camera. The aperture of a lens affects the quantity of light flowing through the lens per unit of time. A larger aperture causes a more shallow depth of field and sharpness. A smaller aperture allows less light to pass through the lens but results in a larger depth of field and sharpness. The main problem with taking pictures of the sun is that inside the solar disc, the intensity is excessively high whereas the circumsolar area has a comparatively low intensity.

Optical systems cannot reproduce perfect images, because there is always some form of distortion or aberration. If the lens system is carefully designed for a particular application, these errors can be minimized. Among the different forms of aberrations and imperfections in the image formation are: spherical aberration, coma, chromatic aberration, astigmatism, distortion or curvature of field. The most important ones for this thesis are explained below:

Spherical aberration: This phenomenon takes place, when the incoming light rays are parallel to the optical axis but at different distances away from it. The outgoing light rays are focused at different points after crossing a spherical surface. Light rays which are further away from the optical axis have a smaller back focal length than the ones closer to the optical axis (see Figure 31). This results in less sharper images and can be corrected by non-spherical lenses.
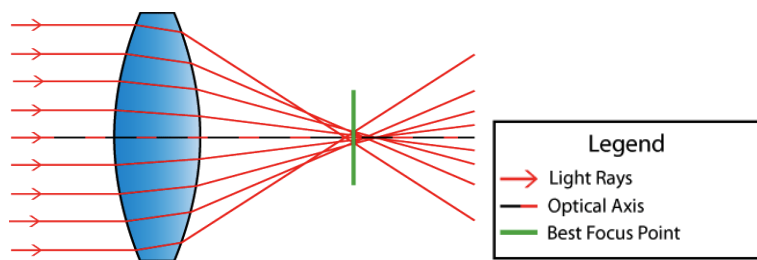
Figure 32: spherical aberration /24/

Coma: This form of aberration occurs due to imperfection in the lens, resulting in off-axis point sources appearing distorted (see Figure 33). It is a superposition of two forms of aberration, namely astigmatism and spherical aberration. In refractive or diffractive optical systems, especially those imaging a wide spectral range (like the sun), coma can be a function of the wavelength, in which case it is a form of chromatic aberration.

Coma can be minimized or eliminated by finding the curvature of the lens surfaces to match the application. /25/
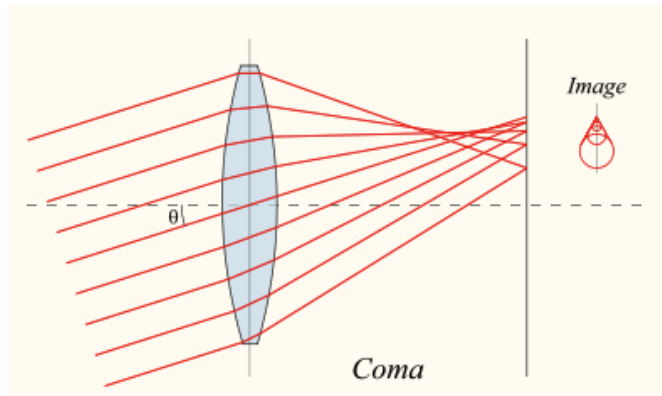
Figure 33: Coma aberration /26/

9.2 CCD Sensor

A charge-coupled device (CCD) is an integrated circuit, which contains a number of linked capacitors. These capacitor arrays are also called photosites, where each represents a pixel in the picture. CCD detectors are based on the photoelectric effect. Incident photons generate electrons by interacting with a semiconductor material. The capacitor array makes up the photoactive region, onto which an image is projected, usually through a lens. The capacitor array is composed of photosites, which accumulate an electric charge proportional to the intensity of the incoming photons. Then a control circuit transfers the charge from one capacitor to the next inside the array. The last capacitor transfers all of its charge into an amplifier, which converts the charge into a voltage signal. This process is repeated until the complete content of the array is converted into a series of voltages. Finally, a digital device samples, digitalizes and stores these voltages inside a memory. CCD sensors can only measure light intensities, in order to obtain polychromatic information, filters have to be used.

The use of CCD sensors in astronomy is common because they can be used for a wide part of the electromagnetic spectrum. This makes CCD devices very useful in the work for this thesis, because the solar spectrum is very broad, and it is necessary to capture a large part of it in order to make significant statements about properties of the sun.

The camera used in the work for this thesis was a Stingray F-504, which works with a CCD sensor. It is manufactured by the company "Allied Vision Technologies", and can be seen in Figure 34. In the chart below, the technical characteristics of the camera are given.

Figure 34: Stingray F-504 /27/

Interface	IEEE 1394b - 800 Mb/s, 2 ports, daisy-chain, fiberoptic (GOF) optional
Resolution	2452 x 2056
Sensor	Sony ICX655
Sensortype	CCD Progressive
Sensorsize	Type 2/3
Cellsize	3.45 μm
Lens mount	C
Max framerate at full resolution	9 fps
A/D	14 bit
On-board FIFO	64 MB

Table 3 : technical specifications of the Stingray F-504 /27/

In addition to the distortions of the telephoto lens, the CCD sensor also has some distortions that can appear in the images. The most typical are the following:

Blooming: This effect appears when pictures of very bright objects are captured with a CCD sensor. Each pixel has a limited charge storage capacity. If this limit is reached, the charge flows to its neighbour resulting in misinformation in the final image. This effect is often observed in pictures with very dark edges next to very bright edges.

The blooming effect can be minimized with "anti-blooming gates", which serve as a drainage channels, where the excess charge can flow away.

Smear: In CCD sensors with interlineal charge transfer, the signal of each line of pixels is transferred vertically through a dark area in between these lines. Due to diffraction or scattering, light of a very bright body can extend into the dark transport region. The erroneous information is added to the image during the read-out of the pixel lines, after the exposure is finished. This causes bright lines to appear vertically in the vicinity of intense light sources. A mechanical shutter can prevent this effect, as it prevents light from reaching the sensor during the read-out of the pixels. In Fig. 35 this effect can be seen clearly.
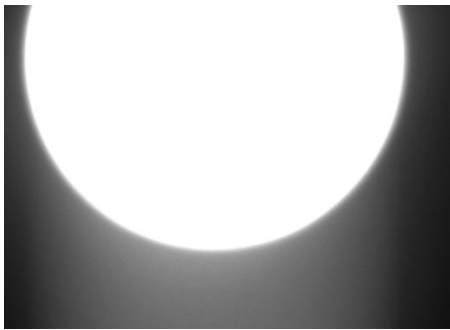
Figure 35: picture taken with the camera Stingray F-504 on 29/11/2011

The camera was connected to the computer by Firewire, which can transfer up to 800 Mb/s. The data was managed by the software Allied Vision, the same company that manufactures the camera.

10. Measurements:

In the following chapter the measurements taken with the ceilometer, the weather station, the aerosol spectrometer and the CCD camera, in eight different situations, are going to be exposed. The chapter is divided in two different parts: in the first one, all the measurements are going to be listed and commented, and in the second one, the relations between these measurements are going to be studied.

10.1 Results of the measurements

10.1.1. 14th of December 2011 at 13:31 h
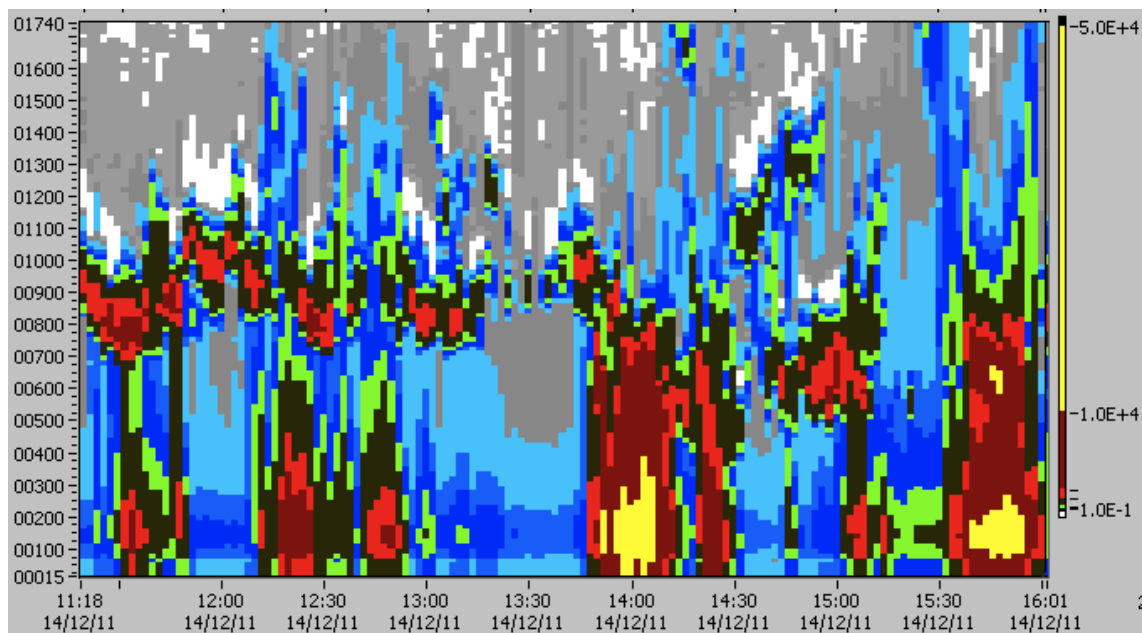
Figure 36: CHM 15K data on December 14th: rainy day, at noontime the clouds broke up and the sun shot out for a short time

In the figure 36 and in the following figures showing the data of the CHM 15K, one can observe three different parameters. The left vertical axis shows the height; in the case of the figure 36 one can observe from 15 meters to 1740. The horizontal axis shows the date and time. The legend situated at the right shows the aerosol particle concentration in the

air. This data is given by the LIDAR and consists in the quantity of photons per time back-scattered by the aerosol particles. /21/

The 14th of December was a rainy day with a very cloudy sky and a varied concentration of aerosol particles and raindrops at a height under 500 m above ground level (see figure 36). The exact time at which the first photo was taken with the CCD camera was at 13:31 h. At this time, the concentration of particles close to ground level, were the lowest of the day. There were some clouds in the sky, but just at 13:31, there was direct solar radiation for a few minutes while at the same time the sunlight was scattered or reflected by the clouds. As there were also some clouds at a height of 3000 m, however thinner than the ones in the figure 36, the weather station registered a high value of diffuse radiation. In the morning there had been some rain, and during the 3 hours before the photo was taken it rained 1.5 mm. The rain gauge recorded 3 mm for the last 24 hours and 13 mm for the last 3 days. This could explain why there was such a low level of particles close to the ground level at the time the picture was taken, because the raindrops pull down the aerosol particles from the air to the ground. In the following table some data from the weather station around 13:31 h is listed. As it can be observed, at 13:30 h the direct radiation was lower, which means that there were clouds in the sky at this time. The low pressure illustrates why the weather was so unstable.

Time (hh:mm:ss)	RH (%)	GR (W/m2)	DirR (W/m2)	DifR (W/m2)	RP (hPa)	T (ºC)
13:30:00	70.774	229.534	294.625	123.255	983.03	8.98
13:31:00	70.496	285.444	583.33	127.044	982.98	9.124
13:32:00	70.366	280.953	584.697	126.593	982.98	9.24

Table 4: Weather data on December 14th

The quantities of the aerosol particles measured on the ground level were very low, as it can be seen in the figure 37. The exact values at the time of the picture, recorded with the Fidas 200®, are shown in the table below the chart.

As it appears in the chart there were some peaks with quantities of almost twenty times more particles with only a few minutes difference. This can happen due to many factors and normally only close to ground level, as a result of the big size of the particles. The representative data should be an average of the data around the time the photo was taken and

Analysis of aerosol particles for the determination of energy losses in solar power plants

of the measurements of the ceilometer. With this, one can be see how high the concentration of particles in low levels of the troposphere is.
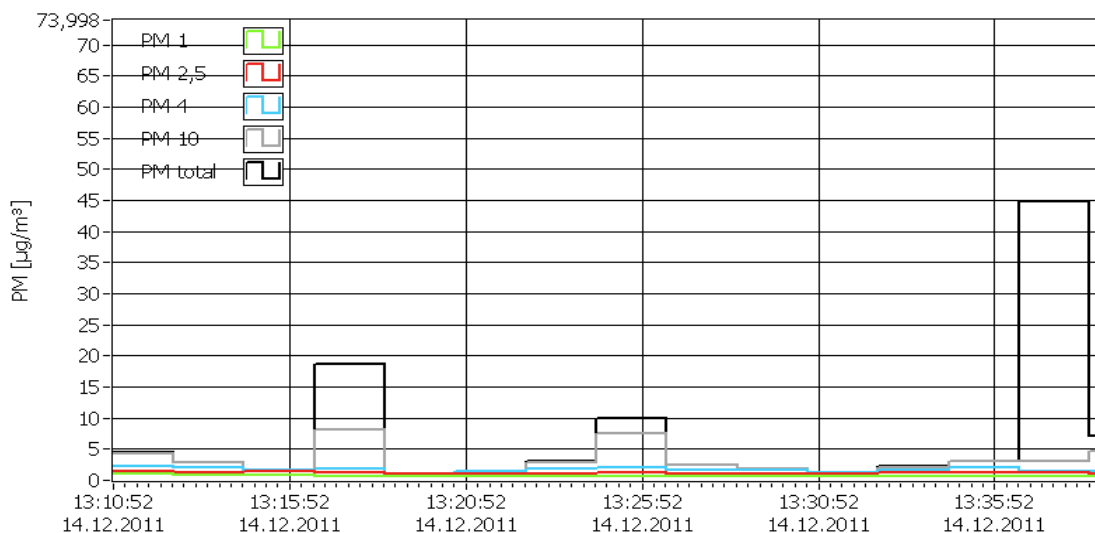
Figure 37: Particles concentration on December 14th

Time	PM 1	PM 2,5	PM 4	PM 10	PM Total
13:28:33	0.6	0.96	1.53	2.46	2.46
13:30:33	0.64	1.02	1.57	1.88	1.88
13:32:34	0.6	0.92	1.23	1.29	1.29

Table 5: Particles concentration on December 14th

Finally, the only measurement remaining is the one of the CSR. This measurement is the most important one, but it is also the most difficult to measure. It was not possible to get an exact value of the CSR due to some problems with the devices used. These problems are explained more in detail in chapter 10.2, in the section concerning the comparison of the measurements. Since it cannot be considered as exact, in this chapter, the measurement of the CSR is thus going to be referred as "relative CSR".

In the following chart, one can observe how high the intensity of the sun light in the photo is. It can also be perceived how, outside of the solar disc, the relative intensity decreases very fast, which means that the relative CRS is low. The result of the relative CSR measurement was 22.64%.
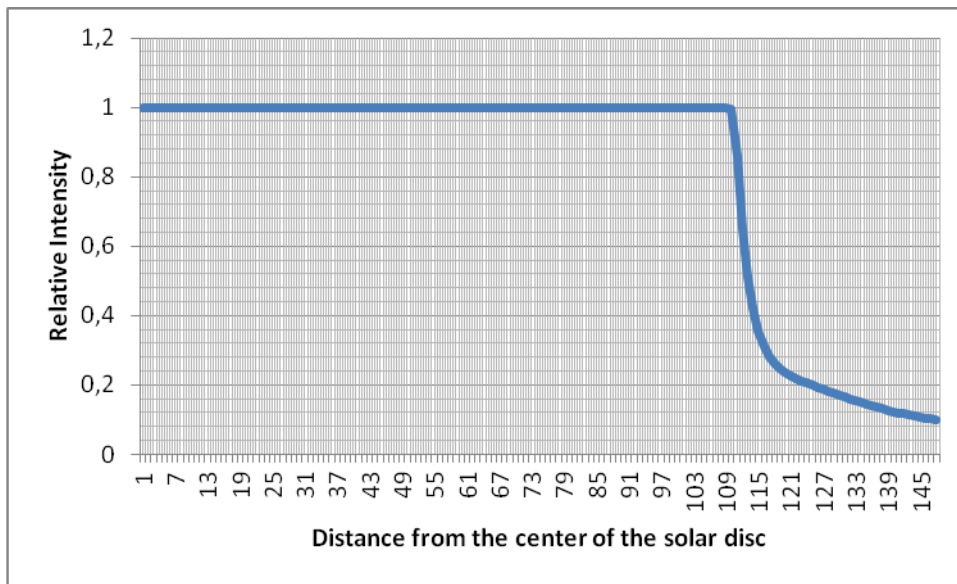
Figure 38: Relative intensity of the sun on December 14th

10.1.2. 10th of January 2012 at 14:03 h
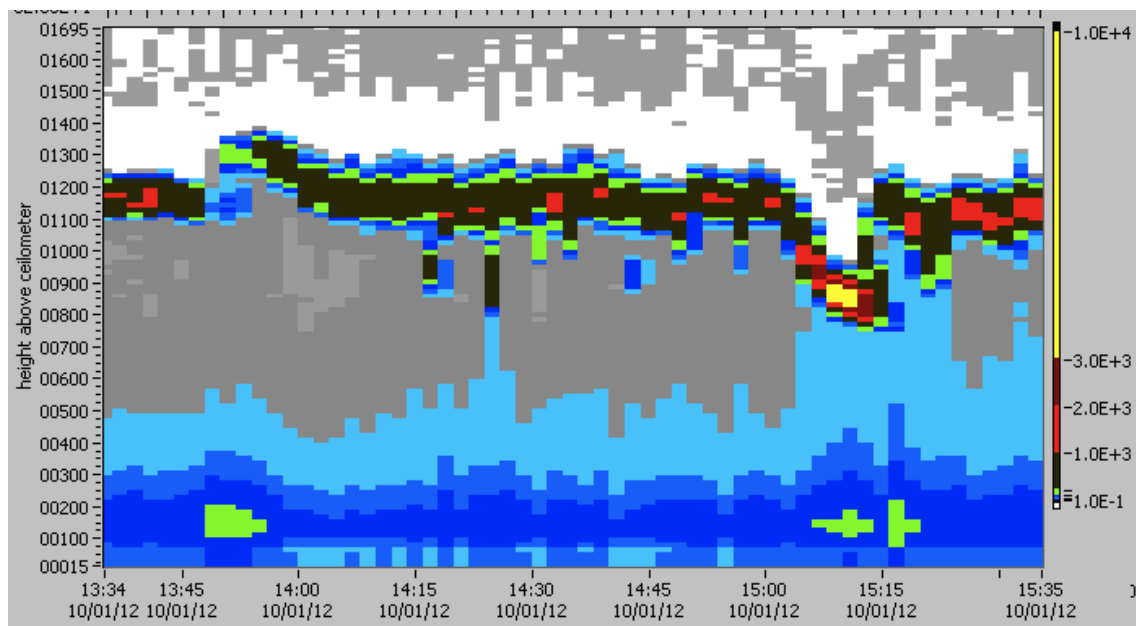
Figure 39: CHM 15K data on January 10th: cloudy day with a high relative humidity

January 10th was a cloudy day but there was no rain. The last time it had rained was the day before with a quantity of 2 mm between 21:00 h and 23:00 h. The last three days there had been 5 mm of rain, and in the previous week about 20 mm. The clouds were situated at a height of 1200 m but the sky was very clear in higher levels of the troposphere. The clouds were not thick enough to reflect all the sunlight, so there was a high amount of diffuse radiation. As it can be gathered from the illustration above, around 14:03 h there was

not a high level of particles close to ground level. The following table lists some of the measurements from the weather station. The variation among the measurements of the direct radiation indicates the presence of some clouds at this time.

Time (hh:mm:ss)	RH (%)	GR (W/m2)	DirR (W/m2)	DifR (W/m2)	RP (hPa)	T (ºC)
14:02:00	73.419	272.294	548.987	104.159	1019.579	9.25
14:03:00	73.659	263.063	527.73	98.94	1019.583	9.304
14:04:00	72.764	263.484	570.815	93	1019.569	9.233

Table 6: Weather data on January 10th

The quantities of particles on the ground level measured with the aerosol spectrometer were higher than on the 14th of December, but they were still low. The following diagram and table show the exact data of the concentration of the particles.
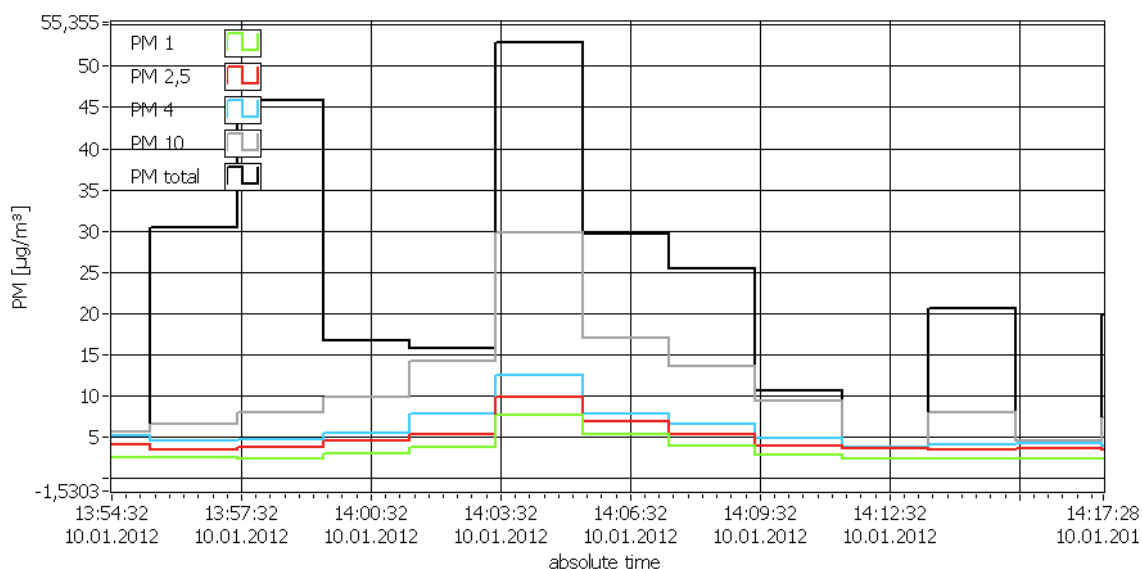
Figure 40: Particles concentration on January 10th

Time	PM 1	PM 2,5	PM 4	PM 10	PM Total
14:01:26	2.96	4.49	5.51	9.9	9.9
14:03:26	3.78	5.27	7.77	14.14	14.14
14:05:26	7.59	9.86	12.57	29.86	29.86

Table 7: Particles concentration on January 10th

Finally, the graph below shows the data of the relative CSR, which seems to be lower than on December 14th, but this will be analyzed more in detail later. The calculated data of the relative CSR was 22.04.
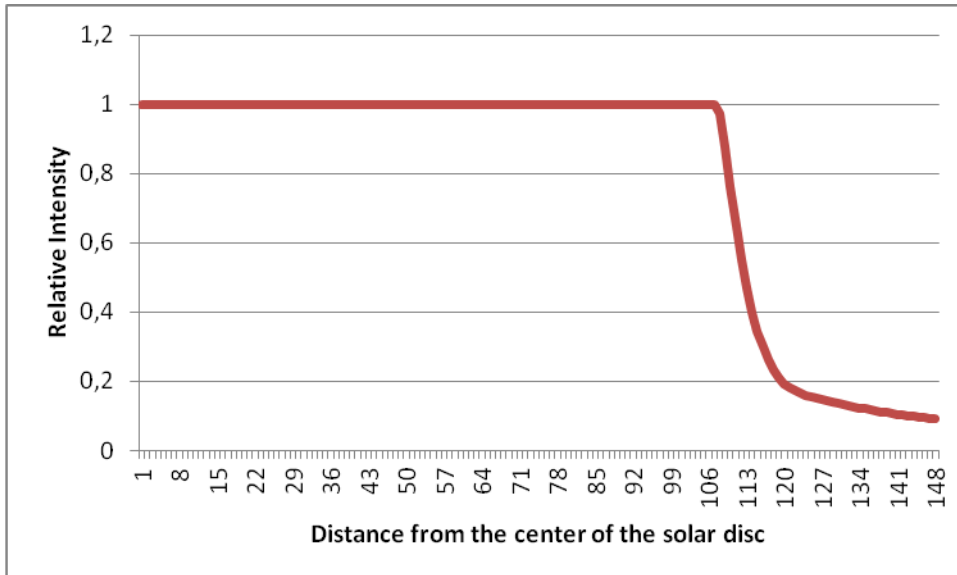
Figure 41: Relative intensity of the sun on January 10th

10.1.3. 11th of January 2012 at 11:34 h
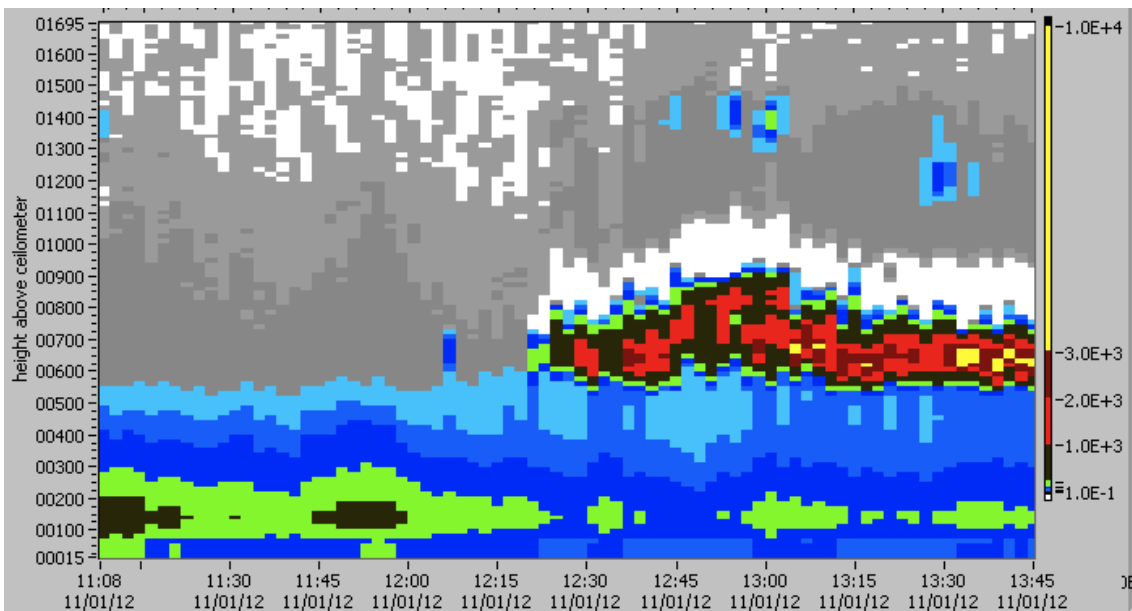
Figure 42: CHM 15K data on January 11th: clear sky with thin stratus clouds and with a higher concentration of aerosols and a higher relative humidity in the lower atmosphere

---

January 11th was a cloudy day, but without rain. The last rainfall had been the night of January 9th, which explains the higher concentration of aerosols at a height between 75 and 300 m in this case. In the morning, at 11:30 h, the sky was really clear, but there were some thin stratus at a height of 7000 m. They are clearly visible in the pictures below. The first one is an image of the ceilometer, which allows observing the atmosphere up to a height of 12480 m. The second illustration is a photo, which was taken with a 3-megapixel camera. It shows how the stratus covered the sun, but also that they weren't thick enough to reflect all of the direct radiation.
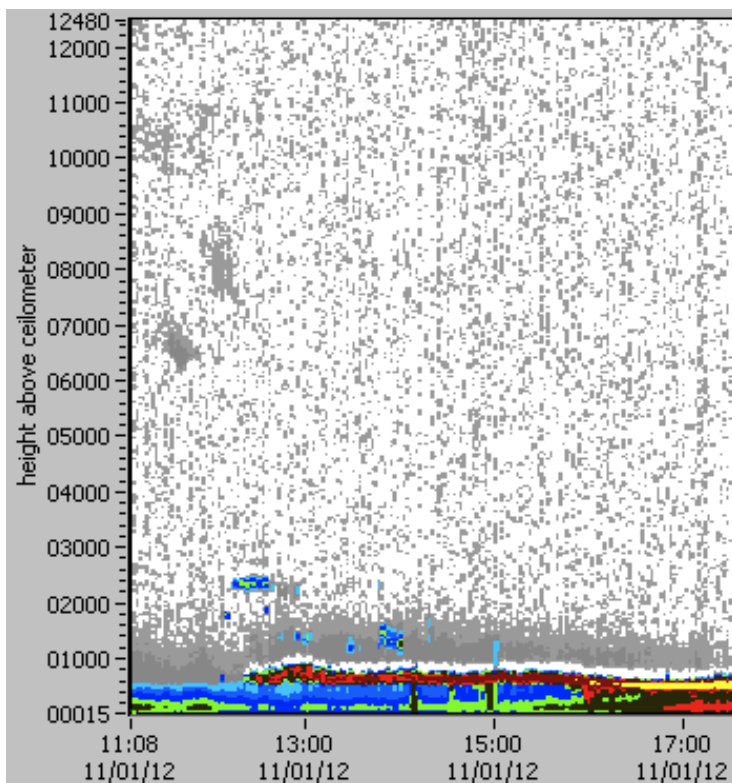
Figure 43: CHM15 k on 11th January

Figure 44: The sky with stratus clouds on January 11th

The presence of these stratus clouds can explain the lower level of direct radiation in comparison to the other measurements, which show cases of cloudy skies but no presence of clouds between the camera and the solar disc. The stratus clouds were very thin and they scattered and reflected the sunlight, but not as much as the wider clouds of the previous days, so the diffuse radiation was not very high in comparison. There was a higher relative humidity, which also has an influence on the solar radiation. The following table lists the weather data around 11:34 h:

Time (hh:mm:ss)	RH (%)	GR (W/m2)	DirR (W/m2)	DifR (W/m2)	RP (hPa)	T (ºC)
11:33:00	80.509	207.979	461.706	41.112	1019.663	9.627
11:34:00	80.395	214.175	474.665	42.219	1019.685	9.768
11:35:00	79.602	216.49	475.897	43.52	1019.677	9.731

Table 8: Weather data on January 10th

The measurements took by the Fidas 200® can be observed in the following chart. The exact data at the time of the picture are shown in the table below the chart.

The amount of small aerosol particles measured close to ground level was quite constant. The measurements of the particles bigger than 4 PM showed extreme differences, suddenly rising to a peak and then decreasing again within a few minutes time.
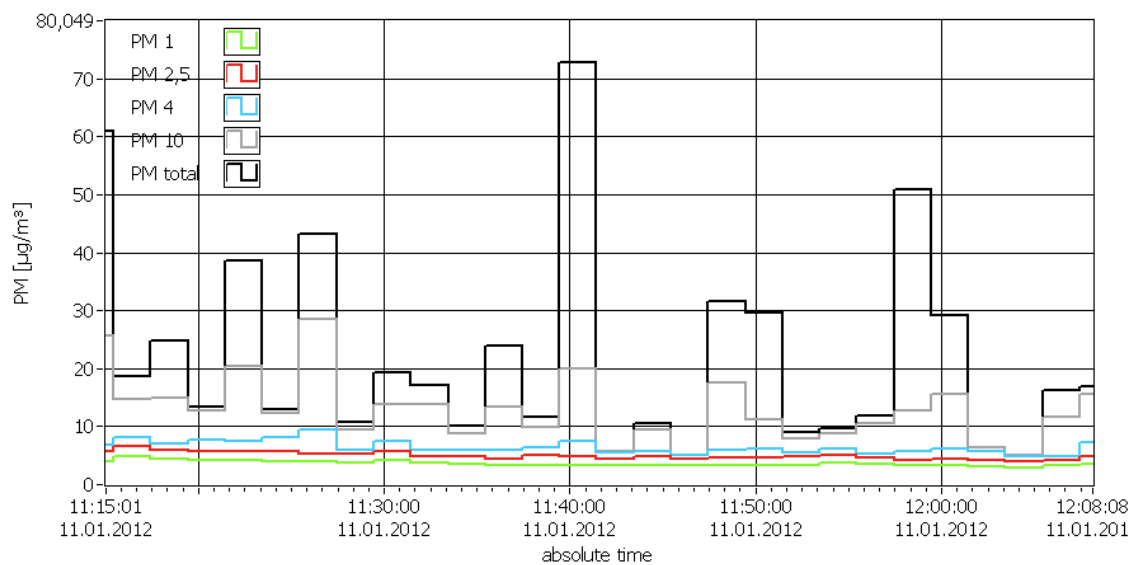
Figure 45: Particles concentration on January 11th

Analysis of aerosol particles for the determination of energy losses in solar power plants

Time	PM 1	PM 2,5	PM 4	PM 10	PM Total
11:31:26	4.09	5.69	7.38	13.9	13.9
11:33:26	3.72	4.83	5.86	13.73	13.73
11:35:26	3.42	4.91	5.95	8.87	8.87

Table 9: Particles concentration on January 11th

The last measurement collected from this photo was the relative CSR. The calculations resulted in 24.39. The diagram below shows the variation of the relative intensity around the sun.
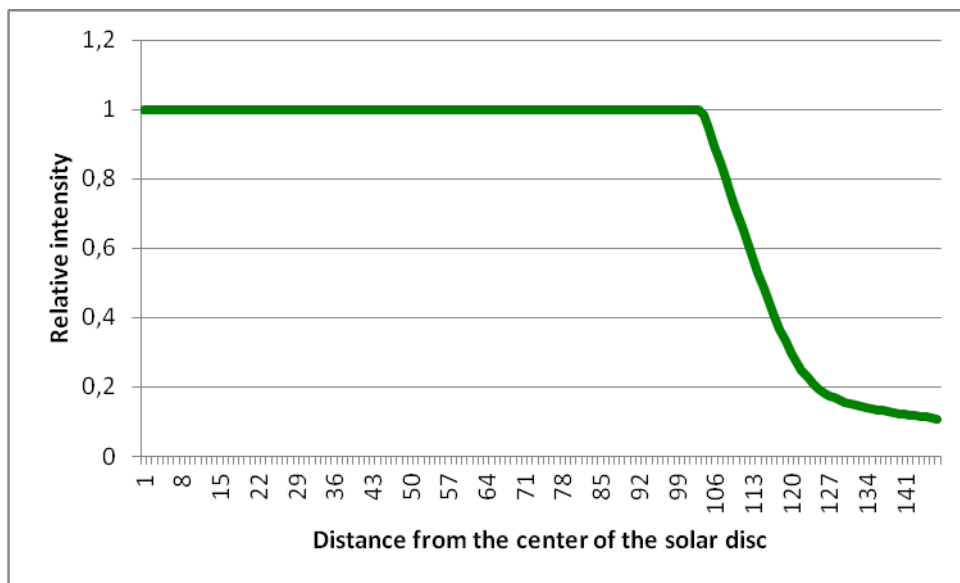
Figure 46: Relative intensity of the sun on December 11th

10.1.4. 13th of January 2011 at 11:06 h and 12:17 h
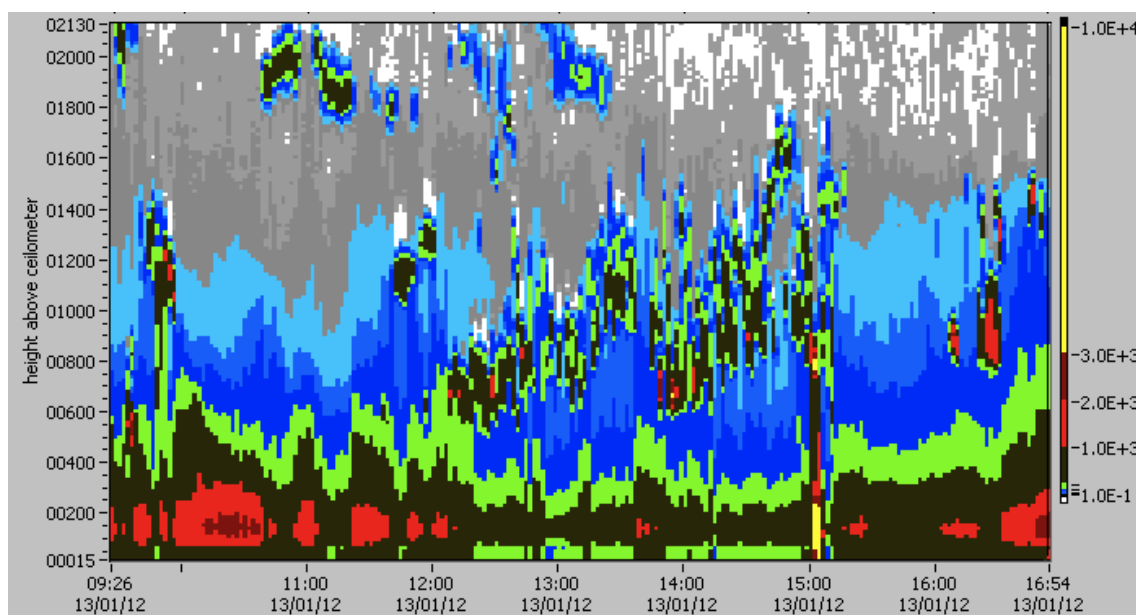
Figure 47: CHM 15K on January 13th: cloudy day with a higher concentration of aerosols and a higher relative humidity in the lower atmosphere

On the 13th of January, two different measurements were taken, one at 11:06 h and the other at 12:17 h. As can be seen in the figure xxx, there was a high concentration of particles in the mornig close to the ground level; part of these particles probably were water molecules, since there was a high amount of relative humidity at this time. At 08:20 h it had rained 0,3mm, but only during 4 minutes, so it is not something that could have an impact on the air composition for the rest of the day. The previous days the weather was dry, with the last rain on the 9th of January. The 13th of January was a cloudy day, which is especially obvious in the second measurement. At the time of the first measurement there were clouds at a height arround 2000 m and at the time of the second one they were lower, between 600 and 1200 m. This explains the high level of diffuse radiation that can be observed in the data recorded by the weather station, which is listed in the table below.

Time (hh:mm:ss)	RH (%)	GR (W/m2)	DirR (W/m2)	DifR (W/m2)	RP (hPa)	T (ºC)
11:05:00	84.854	200.029	554.394	51.432	1013.964	5.282
11:06:00	84.443	206.23	554.971	56.26	1014	5.25
11:07:00	84.255	209.255	433.799	63.89	1014	5.229

12:16:00	77.319	297.199	479.256	104.262	1013.996	5.858
12:17:00	77.065	301.117	464.247	103.385	1013.992	5.94
12:18:00	77.257	300.555	560.065	104.356	1014.008	6.002

Table 10: Weather data on January 13th

In the diagram of the aerosol spectrometer, one can observe a higher amount of small particles than in the previous days, as well as large differences with several peaks of the concentration of particles with a size of more than 2.5 PM. Around 10:30 h one could find the largest quantities of aerosols, which decreased later. In the table below the diagram the exact data is listed.
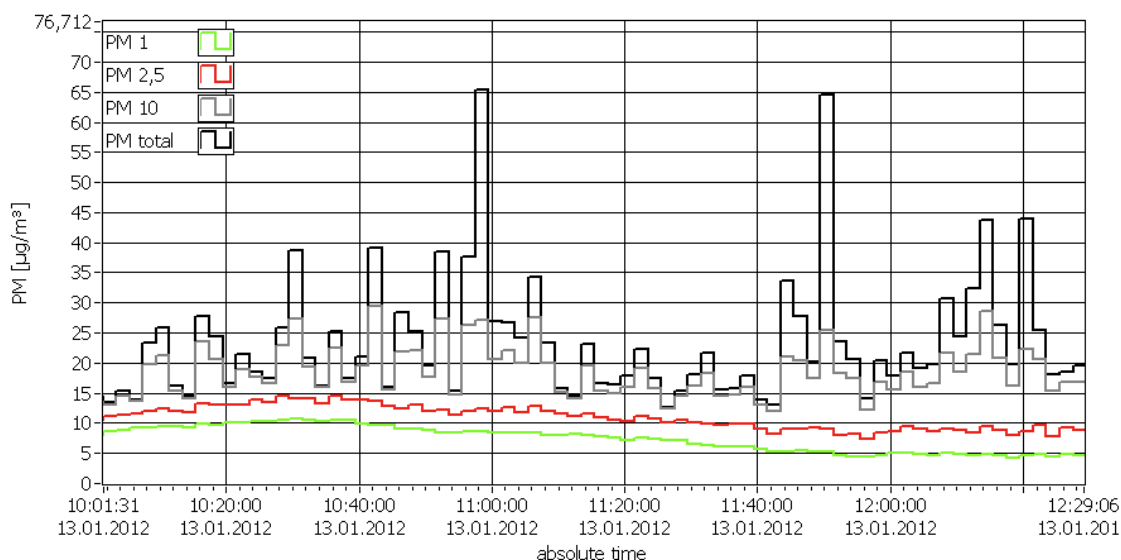
Figure 48: Particles concentration on January 13th

Time	PM 1	PM 2,5	PM 10	PM Total
11:03:29	8.41	12.57	22.09	26.64
11:05:28	8.33	11.83	19.98	24.12
11:07:29	8.39	12.92	27.61	34.26
12:15:29	4.82	9.50	28.63	43.70
12:17:29	4.61	8.88	20.86	26.25
12:19:29	4.26	8.02	19.09	19.67

Table 11: Particles concentration on January 13th

Analysis of aerosol particles for the determination of energy losses in solar power plants

After having examined all the atmospheric conditions with the previous measurements, the relative CSR data at the time the pictures were taken will now be analyzed. At 11:06 h the value was 32.9 and at 12:17 h it was 33.64. The two lines of the graph illustrate the relative intensity of the sun in the two measurements. It was, as it is clearly visible, very similar at both times.
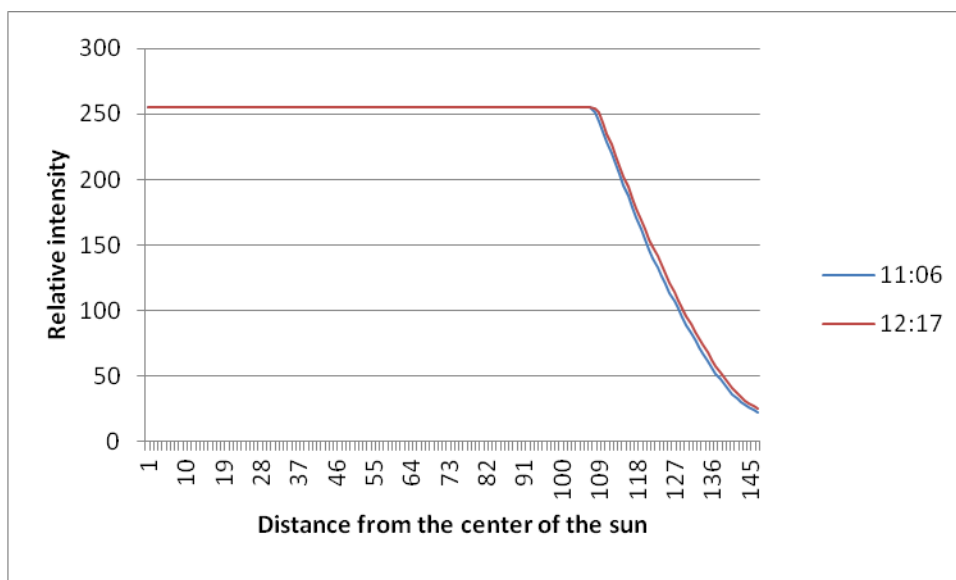
Figure 49: Relative intensity of the sun on January 13th

10.1.5. 16th of January 2012 at 12:15 h, 12:45 h and 14:45 h
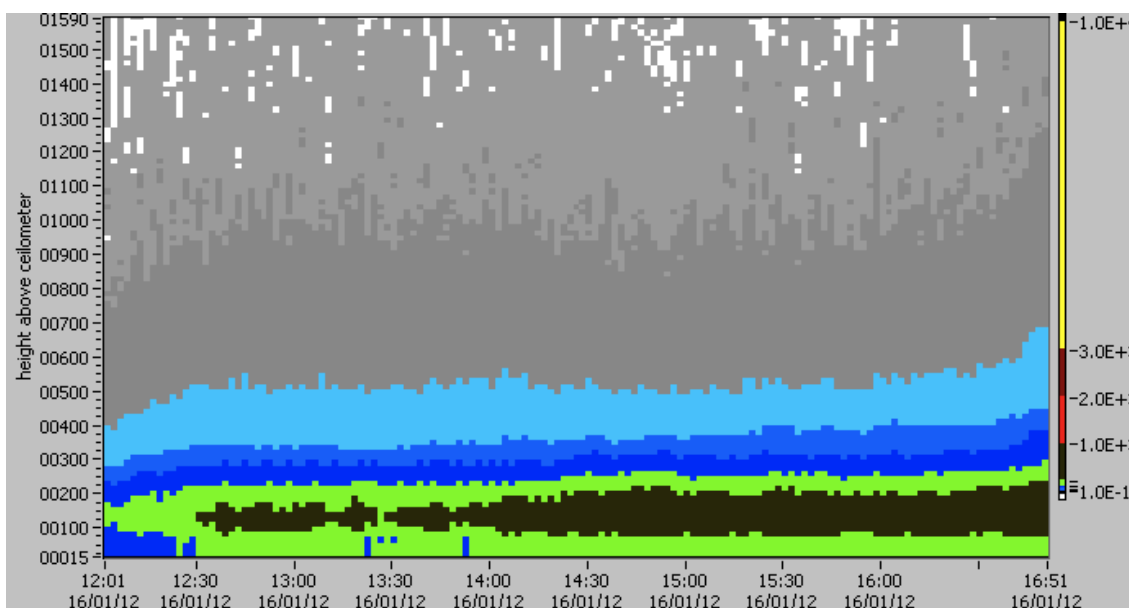
Figure 50: CHM 15K data on January 16th: sunny day with a low relative humidity and a high concentration of particles at the lower atmosphere

Analysis of aerosol particles for the determination of energy losses in solar power plants

The 16th of January was a very sunny day. There weren't any clouds in the sky during the whole day. It was also dry, the relative humidity being much lower than on the other days. The last time it had rained had been in the evening of the 13th of January, but only 0.3 mm. In the previous 7 days the quantity of rain had been below 1 mm, so there was no influence of water drops on the aerosol particles floating in the air. As can be seen in the image from the ceilometer, there was a high concentration of particles in heights between 100 m and 200 m. Since the sky was so clear, the value of the diffuse radiation was very low. The measurements were taken at three different times: 12:15 h, 12:45 h and 14:45 h. The weather was similar at all three different moments, but at 12:45 h there was an increase of the humidity and a decrease of the temperature. In the following table this information is detailed.

Time (hh:ss:mm)	RH (%)	GR (W/m2)	DirR (W/m2)	DifR (W/m2)	RP (hPa)	T (ºC)
12:13:00	51.167	238.39	724.067	6.822	1013.8	4.306
12:14:00	50.361	236.156	713.018	8.144	1013.79	4.292
12:15:00	51.32	241.556	736.292	7.552	1013.8	4.464
12:44:00	71.107	255.251	761.776	10.79	1013.65	2.82
12:45:00	70.968	255.206	761.934	10.941	1013.646	2.773
12:46:00	71.217	254.917	763.186	10.473	1013.65	2.865
14:44:00	58.308	166.929	630.58	0	1013.21	5.47
14:45:00	58.644	165.67	628.814	0	1013.219	5.669
14:46:00	57.537	163.921	625.471	0	1013.229	5.759

Table 12: Weather data on January 16th

In regard to the aerosol particles in the air, in the following graph one can clearly see that the amount of particles is much bigger than it had been on previous days. For the most part of the day, there were near to 20µg/m3 of particles with a size smaller than PM 1, and also some particles of sizes between PM 1 and PM 2.5. The quantities of large particles varied once again, but this time they were higher amounts, with near to 140 µm/m3 as

Analysis of aerosol particles for the determination of energy losses in solar power plants

a maximum. The graph is followed by a table, which shows the exact data at the time of the measurements.
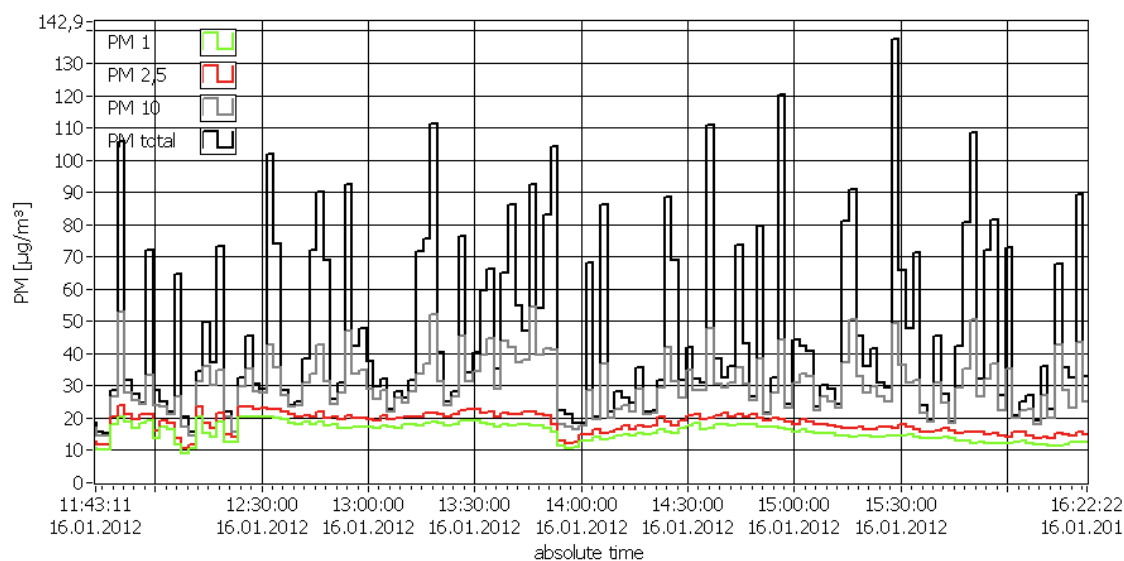
Figure 51: Particles concentration on January 16th

Time	PM 1	PM 2,5	PM 10	PM Total
12:13:28	20.17	23.40	31.30	34.44
12:15:29	15.38	18.23	35.98	49.84
12:17:29	13.96	16.82	30.26	37.31
12:43:29	18.67	20.91	30.89	38.54
12:45:29	17.97	20.32	33.59	71.86
12:47:30	18.67	22.10	42.83	90.07
14:43:30	17.52	20.46	30.76	36.15
14:45:29	17.94	21.06	35.61	73.69
14:47:28	18.02	20.52	30.51	43.07

Table 13: Particles concentration on January 16th

Finally there are measurements of the value of the relative CSR. On January 16th there were the highest values of relative CSR. As it is seen in the following graphic the values were very similar, at 12:15 h and 12:45 h they were more or less the same value, as it is in graphic, where both lines follow the same way. Relative CSR has been calculated as

39.31 and 39.58 respectively. At 14:45 h the intensity of the sun was lower, but in the graphic the curve is similar than the others, this happened because the weather and air conditions were similar. The value of relative CSR here was 35.31.
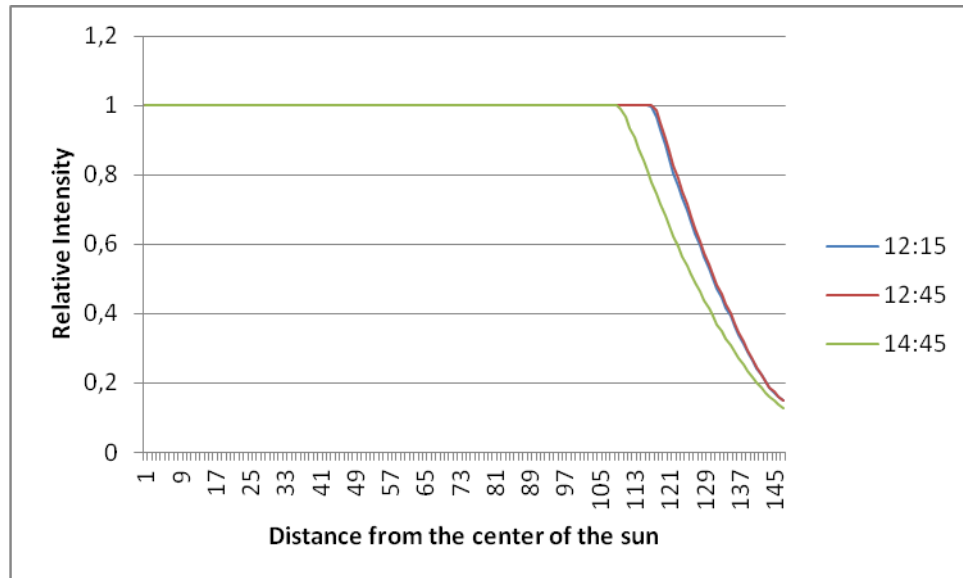
Figure 52: Relative intensity of the sun on January 16th

10.2. Relation between the measurements:

In the following pages, the different measurements which were taken are going to be compared and analysed. All the collected data will be included in this analysis in order to identify which measurement has an impact on the relative CSR.

As has already been mentioned in the beginning of the chapter, the CSR is referred to as relative CSR because the devices used for the measurements of this thesis could not provide the accurate data necessary for calculating the exact CSR.

The first problem, which makes the measurements inexact, is the light in the sky that is not part of the direct radiation. The CCD sensor captures light from the dark sky behind the sun and from the diffuse radiation, so this light should not be included in the circumsolar radiation or in the sun radiation. If this radiation is not considered the calculated CSR will be higher than the real one, that is because the intensity inside the solar disc is not influenced by this radiation (is already the maximum that the sensor can measure), but it is added to the circumsolar area's light.

Analysis of aerosol particles for the determination of energy losses in solar power plants

The size of the sun in the pictures is another problem found in the measurements. The entire sun diameter was inside the picture; its diameter measures 1227.26 pixels and the length measured by the program is 1748 pixels. As one can observe in the figures where is shown the relative intensity of the sun, the intensity is still decreasing at the end of the measurements, which means that there is light from the circumsolar radiation that is not included in the calculated CSR. That makes an estimated CSR lower than the real one.

As has been written in previous chapters, the intensity of the sun should be higher in the area around the centre of the sun than at the outer edge of the solar disc. However, the measurements taken for the research of this thesis list a constant data for the entire solar disc, which means that the calculated data of the CSR might be imprecise. But by observing the changes in the circumsolar area one should be able to come to significant conclusions all the same.

The direct radiation measured by the pyrheliometer refers to the direct radiation plus the radiation of the circumsolar area, which is why the total intensity recorded with the CCD sensor, should be related to this data. The following table lists the measurements of the direct radiation and of the diameter of the circle with maximum intensity, taken at the same time.

Day	Diameter (pixels)	Direct Radiation (Wm-2)
December 14th	649	584
January 10th	631	550
January 11th	613	474
January 13th (11:06)	631	554
January 13th (12:17 h)	637	560
January 16th (12:15 h)	691	730
January 16th (12:45 h)	697	761
January 16th (14:45 h)	640	628

Table 13: Diameters and direct radiation

As one can observe, the diameter of the circle with maximum intensity is normally longer if there is more direct radiation. This influences the relative CSR data because the intensity inside the solar disc should be higher than in the circumsolar area. This makes the relative CSR calculated in the days with high radiation to be higher.

Analysis of aerosol particles for the determination of energy losses in solar power plants

In order to compare the data, it is necessary to keep in mind that there are other factors that could change the intensity of the sun. They will be commented on later.

As can be seen, the data follows a logical order, linking the intensities and the diameters. However, there is one exception, which becomes obvious in the comparison of the 14th of December and the 16th of January. These days were really different; they didn't have any measurement in common; temperature, relative humidity, atmospheric pressure, diffuse radiation, level of particles and relative CSR were different. The following pages will give further details of the comparison of all these factors.

Regarding the temperature, it is similar for most of the days: 2.7ºC being the coldest and 9.7ºC the warmest result. The temperature is important because the maximum level of the absolute humidity depends on it.

The atmospheric pressure affects the weather, but not directly in terms of the amount of direct or indirect radiation. The 14th of December was the only day there was rainy and unstable weather and also low pressure. On the other days, there were high pressures and stable weather.

The relative humidity is more important in relation to its effect on the solar radiation. A higher humidity in the air means that there is also more water vapour, so this water can diffuse the solar radiation. With a higher level of humidity in the air the diffuse radiation should be higher than with a low humidity under the same conditions, which means the same should apply to the relative CSR. In the table below shows the data of the relative CSR, the indirect radiation and the relative humidity.

Day	Intensity diffuse radiation (Wm-2)	Relative humidity (%)	CSR
14th December	127	70.5	22.64
10th January	100	73	22.04
11th January	42	80	24
13th January (11:06 h)	56	84	32.9
13th January (12:17 h)	103	77	33.64
16th January (12:15 h)	7.7	50.6	39.31

16th January (12:45 h)	10.8	71	39.58
16th January (14:45 h)	0	58	35.31

Table 14: data of the relative CSR, the indirect radiation and the relative humidity

The obtained results listed above make it difficult to identify the impact of the relative humidity. But on the 16th of January, there were similar conditions throughout the whole day and, most importantly, there were no clouds in the sky. Between 12:15 h and 12:45 h there was a 20% increase of the relative humidity and it as one can see in the table, the CSR and the diffuse radiation were a bit higher.

Concerning the diffuse radiation and the global radiation, the amount of these radiations will be analyzed, as well as why they exist and if there is any relation between the diffuse and global radiation and the direct radiation.

As has already been said in previous chapters, the sunlight is scattered by small particles in the air. Normally, the majority of the diffuse radiation comes from the direct radiation scattered by the clouds and other aerosols particles. The majority of the clouds that scatter the solar radiation are situated between 800 m and 2000 m. The scattered radiation doesn't only come from the clouds that cover the sun from the point of view of the observer. It also comes from the other clouds that diffuse the light in all directions. When low clouds are covering the sun, part of this diffuse radiation can be registered in the pyrheliometer as direct radiation, because the scattering can be very light, and be part of the circumsolar area. On days with clear skies, there is also some diffuse radiation because the aerosol particles scatter the light as well. The following charts detail the diffuse radiation on the days the measurements were taken, as well as the comparison between diffuse, global and direct radiation on the 11th of January.

In the first chart, the measurements of diffuse radiations of every day are shown. They were not very regular on cloudy days, and when the sky was completely overcast, the diffuse radiation did not exist or was very low due to the high albedo of the clouds. In the second chart, one can see how the different radiations changed in an aligned manner on the 11th of January. When there was no direct radiation, the diffuse was lower, especially when the sky was completely overcast. The global radiation was more constant, but always increased or decreased depending on the amount of direct radiation.
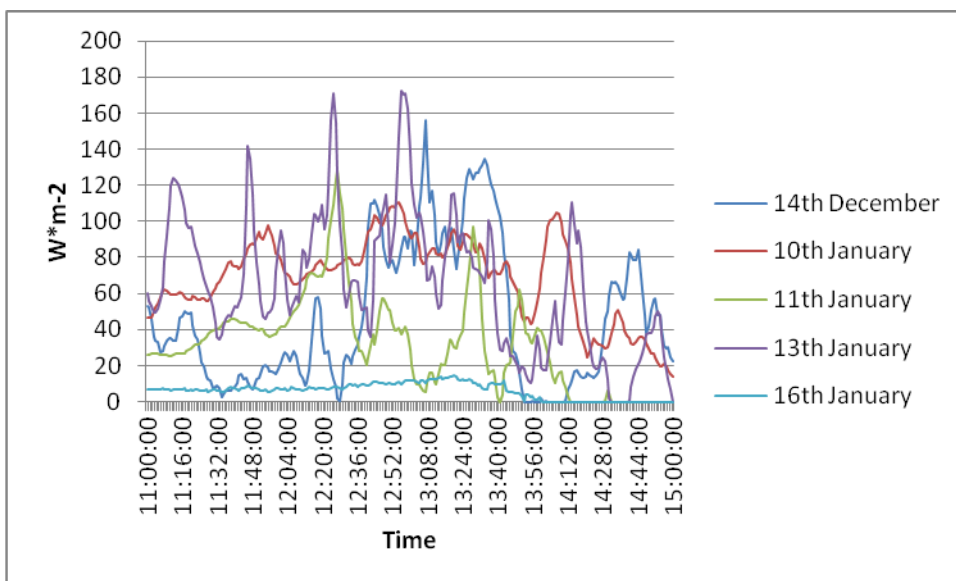
Figure 53: Diffuse radiation each day
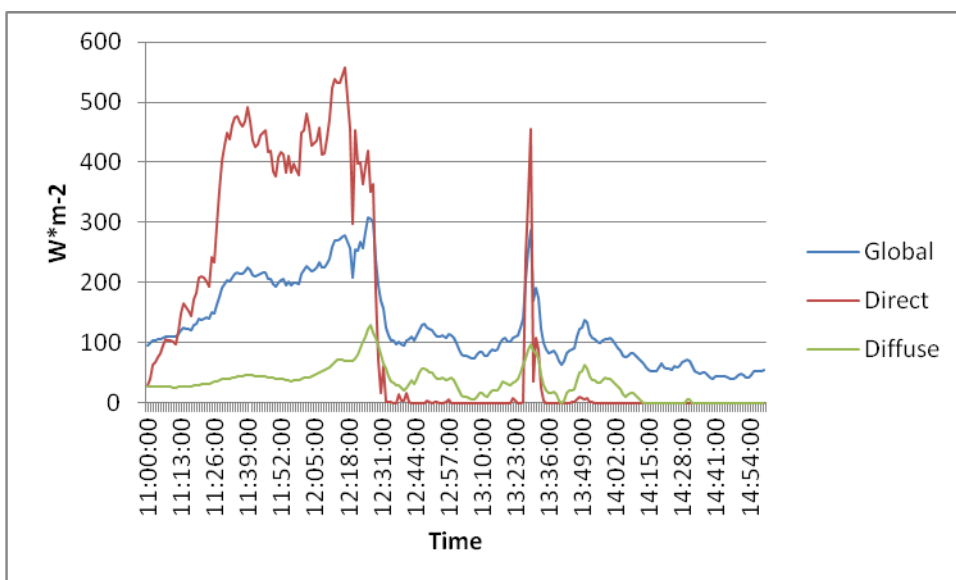
Figure 53: Global, diffuse and direct radiation on 11th of January

Now the relation between aerosol particles and radiation is going to be examined. In order to carry out the research correctly, the weight of the small particles measured has to be separated in coarse and fine particles. As has already been mentioned previously, the particles with the greatest impact on the solar radiation are the small particles, with a size under 2.5 PM. The chart below shows the quantities of particles with a size bigger than 2.5 PM in relation to the global, diffuse and direct radiation on the 16th of January. One can observe that there is no relation between coarse particles and radiation.
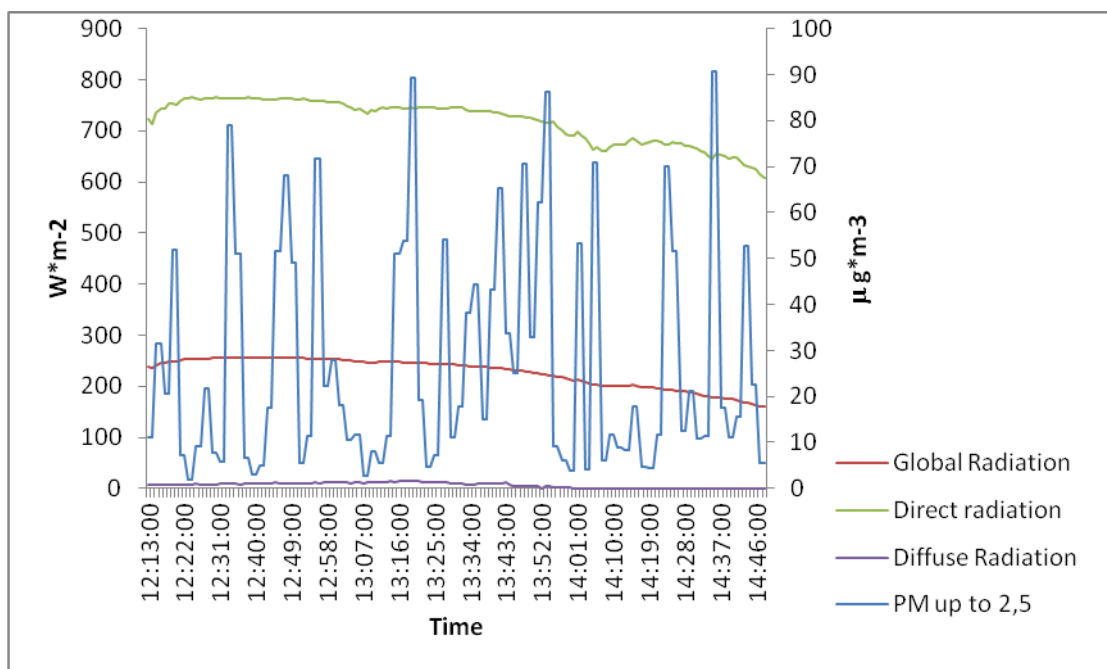
Figure 54: Coarse particles and radiation on January 16th

At 12:15 h, the amount of particles bigger than 2.5 PM was between 10 and 30 µg/m3, and at 12:45 h between 17 and 67 µg/m3. But the calculated data of the relative CSR was very similar: 39.31 and 39.58. While the particle data shows great differences, the concentration being up to 10 times higher at times, this variation does not affect the radiation level. Finally, the following charts illustrate the comparison of the different relative CSR measurements. The different graphs in the diagram below show the variation of the intensity outside of the solar disc in all of the measurements that were taken.
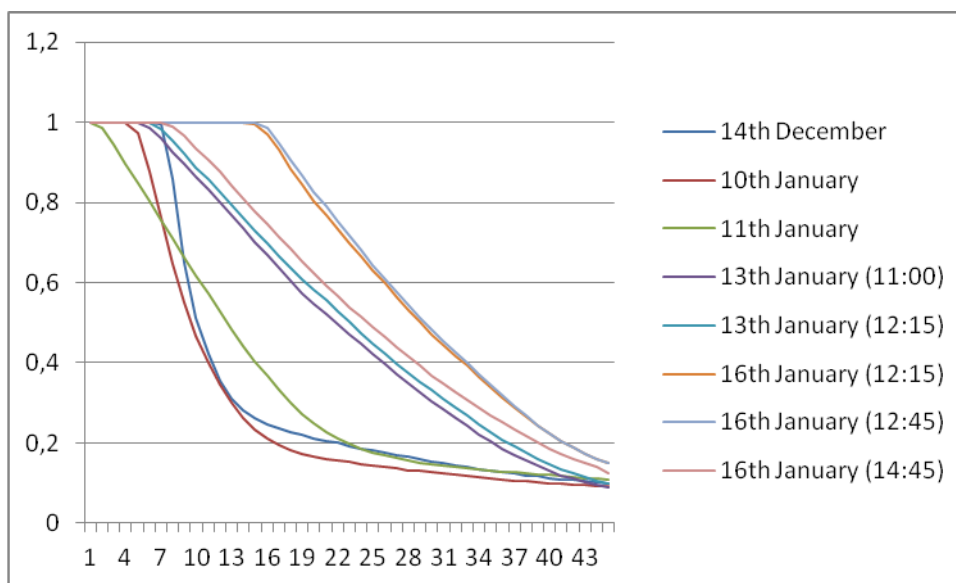
Figure 55: Relative intensity in the circumsolar area each day

Analysis of aerosol particles for the determination of energy losses in solar power plants

At first sight, two different groups can be distinguished: the measurements on days with low particle levels (December 14th, January 10th and January 11th), and the rest, with high levels of particles. The most important difference is the way in which the level of the sun intensity in the circumsolar area decreases. As had been mentioned earlier, the days with more direct radiation had a bigger intensity around the solar disc, but this didn't mean that the relative CSR was bigger. It is thus going to be more representative how the intensity decreases outside of the solar disc.

In the following, the measurements will be taken in pairs and then put in comparison in order to determine these differences. The first comparison will be between the measurements of the 14th of December and the 13th of January at 12:17 h. They have a similar data of direct radiation and also a similar diameter with top intensity, so it is going to be easy to compare them. On the 14th of December the average weight measured of particles under 2.5 PM on the ground level was around 1 µg/m3 and on the 13th of January it was 8,8 µg/m3. The ceilometer measured a concentration of 5-20 below 500 m on December 14th and of 100-220 on January 13th. There was thus a considerable difference between the results. The relative CSR was also very different. In the following table, the variation of the relative intensity can be observed:

Distance (pixels) / Day	December 14th	January 13th (12:17 h)
18	100 %	99.99 %
36	99.59 %	95.97 %
42	85.69 %	95.47 %
48	64.84 %	92.02%
60	42,2 %	83.14 %
72	31.08 %	72.72 %
102	18.66 %	44.72 %
150	14.42 %	26.23 %
228	9.86 %	9.84 %

Table 16: comparison of solar relative intensity in the circumsolar area at December 14th and January 13th

The distance is measured from the border of the solar disc. Around the sun the intensity was relatively the same. One could remark slightly higher numbers on the 14th of December, which decrease very quickly with greater distance to the sun, which indicates a small

CSR. The intensity on the 13th of January, on the other hand, decreases much more slowly, which means that there is a higher CSR.

On the 13th of January at 12:17 h and on the 16th of January at 14:45 h the diameters with maximum intensity were of a similar size. The concentration of small particles on the ground level was very different; on January 13th it was 8,8 µg/m3 and on January 16th it was more than twice as much: 20 µg/m3. Regarding the ceilometer, the concentration on January 13th was between 100 and 220 at a height below 500 m and towards the ground level it became increasingly higher. On the 16th of January the concentration was similar, but the highest levels were above 75 m. The following table shows the relative intensity measured from the border of the solar disc.

Distance (pixels) / Day	13th of January (12:17 h)	16th of January (14:45 h)
32	99.85 %	99.99 %
42	95.37 %	98.37 %
60	85.65 %	90.62 %
90	69.71 %	74.56 %
120	55.55 %	59.33 %
200	20.83 %	25.18 %

Table 17: comparison of solar relative intensity in the circumsolar area between January 16th and January 13th

In this table one can observe that the graphs from the two days in question are quite similar, and that their relative CSR data doesn't vary much from another. The main differences one could highlight are in the solar intensity and in the PM on the ground level.

The next comparison will be between the 10th and the 11th of January. These days were much more similar than the previous ones in relation to the particle levels and the weather conditions. On the 10th of January, the concentration of particles with a size under 2.5 PM on the ground level was measured about 5.5 µg/m3, very similar to that of the 11th of January, which was about 5µm/m3. However, the particle concentration measured by the ceilometer showed some differences. At low heights (below 200 m), the concentration measured on January 10th was between 5 and 40, and on January 11th between 20 and 100. The amount of particles was thus similar at the ground level, but not at a higher levels. One should also not forget to consider the influence of the cirrus clouds at a height around 7000 m on January 11th. The other big difference was in the direct solar radiation, which is

why the length of the diameter with maximum intensity was also different and it was harder to see the variation of the relative CSR between both days. The best way to perceive the variation is by observing the different distances (pixels) in relation to the decreasing intensity. The table below illustrates this and it is clearly visible that the relative CSR is higher on 11th January.

Relative intensity / Day	January 10th	January 11th
100 % to 95%	13 pixels	17 pixels
95% to 90%	4 pixels	6 pixels
90% to 80%	6 pixels	12 pixels
80% to 65%	9 pixels	18 pixels
65% to 50%	9 pixels	18 pixels
50% to 25%	27 pixels	42 pixels
25% to 18%	24 pixels	24 pixels
18% to 10%	120 pixels	120 pixels

Table 18: comparison of the relative solar intensity in the circumsolar area between January 10th and January 11th

 One has to remark that the diameter with maximum intensity on the 10th of January was 18 pixels larger than that on the 11th of January and that this table thus only considers the variation of the light intensity as the measurements were not taken in the exact same place.

11. Conclusion

The main objective of this thesis was to determine the impact of aerosol particles on solar radiation, which has been achieved successfully: the results of the measurements show a clear relation between the quantity of aerosol particles and the relative CSR. However, there were also many problems encountered while carrying out the measurements and calculating the CSR data, which could not solve all during this thesis.

To find the perfect relation between the aerosol particles concentration and the CSR, it is essential to know the exact concentration of particles between the camera and the sun. However, the devices used for the research of this thesis - the CHM 15K and the Fidas 200 - did not allow an exact determination of this data. The ceilometer can only measure in vertical direction, but since the photos had been taken at an angle around 35° the data obtained in these measurements is an approximation of the real one. The aerosol spectrometer measures aerosols at ground level, where the particles scatter very little light. While the concentration of particles at higher levels is similar, it is not exactly the same, especially in the case of the large particles. Moreover, as large particles cause little scatter of the light, they do not have a relevant impact on the CSR at lower heights. The quantity of large particles measured by the Fidas 200 can thus not be considered relevant for the purposes of this thesis.

Nevertheless, the data obtained with both devices allows an approximation of the concentration of particles in the air. With the aerosol spectrometer one should not consider the data of the coarse particles, but the fine particles must be similar next to the ground level. The data obtained using the ceilometer should be alike to the data in a 45° angle, but the thin clouds in upper levels of the atmosphere are normally different. For this reason, when the measurements were taken, the cirrus clouds that covered the sun were noticed. These problems have appeared in all of the measurements. However, since they were all carried out in the same way, the measurements are still suitable for the comparisons.

There are also some distortions that can affect the result of the CSR, which needs to be calculated. The problem found with the intensity of the sun can increase the data of CSR. The sun is brighter in the centre than near the edges of the circle, but due to the technical limitation of the camera, the whole solar circle was measured with the same intensity. Another flaw is the brightness of the sky, which is included in the quantity of light of the circumsolar area, resulting in a higher CSR. Two other distortions can decrease the calculated

data of the CSR: one is the light that is not measured due to its location outside of the picture, and the other one is the circumsolar radiation shining inside the solar disc. As one can observe in the measurements, the size of the photo is not much bigger than the sun. Watching the data obtained by the program Visual Builder one can see that the light is still decreasing at the edge of the measured data, so there is some light that is not included into the circumsolar radiation and it causes a relative CSR smaller than the real one. The last distortion is difficult to be quantified, as well as in the "solar aureole" there is some diffuse radiation inside the solar disc, but it is measured as direct radiation. This distortion therefore causes the CSR to be calculated less than it actually is.

Although it is clear that the relative CSR calculated is not exactly the real one, it is a valid data for the comparison of all the measurements, because the distortions are the same for all of them.

The days in which the measurements were taken had very different meteorological conditions, which were taken into account and compared. However, as one can see in the end, the quantity of aerosols in the atmosphere was the data which influenced the variation of the sun radiation the most.

The German climatology was a further problem during the research of this thesis. In the nearly two months in which the measurements were taken, there were only eleven sunny days, making it difficult to obtain the best data. Finally, the measurements of five different days, in which the atmosphere had distinct conditions, were used for the comparison.

Analyzing the data obtained in detail, one can clearly observe whether there is any influence of the different measured parameters. Meteorological parameters cause a very small influence on the relative CSR calculated. The relative humidity scatters the sunlight, but as one can see in the table 14, its influence is not important. The direct and diffuse radiation also have an influence on the relative CSR (the direct radiation is used to calculate the relative CSR) but with the data obtained one cannot appreciate it clearly. The data of the temperature, or the pressure have an influence on the climatology,therefore the influence exists, but it is indirect. The wind speed and direction have an influence on the aerosol particle concentration in the air, but they also have an indirect influence. However, there is a clear relation between the concentration of the aerosol particles and the relative CSR, especially the small particles. When analyzing the data, one can see how the days with a higher aerosol particle concentration also registered a higher relative CSR. In the tables 16, 17 and 18 and the figure 55, one can see the influence.

After the analysis of the measured data, it can be confirmed that the main objective of the thesis was reached: it proves that the circumsolar radiation is caused by the interaction of solar light and aerosol particles.

The Solar-Institut Jülich has been studying solar radiation for many years. While the circumsolar radiation is a very important part of solar radiation, not many studies have been done about it. This thesis is a first intent of showing the great impact of the aerosols on the solar radiation and it will show the way for further studies and projects in the future. In order to obtain more exact results, one should consider using improved or even different devices.

Nowadays solar thermal energy is developing very fast and the plants are starting to become profitable in places with high solar radiation. It is estimated that in year 2030, 15% of the energy consumed in the European Union will come from North Africa. The ambitious "Desertec" project in North Africa, for example, is close to start construction. This project consists in the construction of many renewable energy plants, mainly solar thermal. These will be located in the Sahara desert, where the aerosol particle concentration is very high. It will therefore be very important to know how much of an impact the aerosol particles have on the solar radiation. In the effort of improving solar thermal energy, which is especially important in times when renewable energy sources are becoming essential, this thesis thus represents a significant contribution, which would be worth continuing.

Bibliography

/1/   Solar-Institut Jülich (2011).

/2/   RWTH Aachen University, Skript zur Vorlesung Energiewirtschaft (2010)

/3/   Emilio, Marcelo; Kuhn, Jeff R.; Bush, Rock; Scholl Isabelle., "Measuring the Solar Radius from Space during the 2003 and 2006 Mercury Transits" (2012).

/4/   International Astronomical Union: "Resolution B2 on the re-definition of the astronomical unit length" (2012).

/5/   National Meteorological Institute of Costa Rica (2009). web: http://www.imm.ac.cr

/6/   The National Institute of Standards and Technology. web: http://www.nist.gov

/7/   Kopp, G.; Lean, J. L., "A new, lower value of total solar irradiance: Evidence and climate significance" (2011).

/8/   Wikipedia/solar spectrum. web:
       http://en.wikipedia.org/wiki/File:Solar_Spectrum.png

/9/   Web Minority Serving Institution Partnership Development Program (2010)
       web: http://www.spacegrant.montana.edu/msiproject/index.html

/10/   Web astronomía: web: http://www.astromia.com/astronomia/rayleighmie.htm

/11/   Observatório Nacional, Brazil (1998-1999)

/12/   D. Buie; A.G. Monger; C.J. Dey., " Sunshape distributions for terrestrial solar simulations" (publication)

/13/   Intergovernmental Panel on Climate Change, " IPCC Third Assessment Report - Climate Change 2001". web:
       http://www.grida.no/publications/other/ipcc_tar/?src=/climate/ipcc_tar/wg1/160.htm

/14/   National Oceanic and Atmospheric administration, web:
       http://commons.wikimedia.org/wiki/File:Mauna_Loa_atmospheric_transmission.png

/15/   Sjaak Slanina. "The Encyclopedia of Earth, Aerosols"
       http://www.eoearth.org/article/Aerosols

/16/   Universidad de Chile, web:
       http://www.atmosfera.cl/HTML/meteorologia/nubes5.htm

/17/   Wikipedia, "albedo", web:
       http://en.wikipedia.org/w/index.php?title=File:Albedo-e_hg.svg&page=1

/18/   NASA Earth observatory, "Clouds&Radiation web:
         http://earthobservatory.nasa.gov/Features/Clouds/

/19/   National Weather Service, "Clouds classification" web:
         http://www.srh.noaa.gov/jetstream/synoptic/clouds_max.htm

/20/   Wandinger, U; "Introduction to lidar, in Lidar - Range-resolved optical remote
         sensing of the atmosphere" (2005)

/21/   Jenoptiks, "CHM 15 k User Manual" web:
         http://www.jenoptik.com/en_50377_chm_15k

/22/   Palas, "Fidas 200 User Manual" web:
         http://www.palas.de/en/product/fidas200

/23/   Walimex, web: http://walimex.nuna.ch/

/24/   Photography life, "What si Spherical Aberration?" web:
         http://photographylife.com/what-is-spherical-aberration

/25/   Gebelein, Rolin J.; David Shafer, "Reflecting telescope with correcting lens" (1986)

/26/   Wikipedia, "Coma aberration" web:
         http://en.wikipedia.org/w/index.php?title=File:Lens-coma.svg&page=1

/27/   Allied Vision Technologies, "Stingray", web:
         http://www.alliedvisiontec.com/emea/products/cameras/firewire/stingray.html

/28/   DC Views, "Blooming Effect", web:
         http://www.dcviews.com/tutors/tt55812.htm

Annex

A1 Calculations

The appendix includes the measurements that were taken in order to calculate the estimated value of the circumsolar ratio.

As has been said in previous chapters, the equation used to calculate the direct beam of the sunlight and the circumsolar radiation depends on the size of the sun and the light intensity. It was thus first of all necessary to know the exact size of the sun in the photos. To make this possible it was required to calibrate the camera.

In order to calibrate the camera, pictures of another object had to be taken. The same focus had to be used for this object as for the sun, so it needed to be located far away. From the roof of the SIJ (the place where the photos of the sun were taken), the tower of a church was visible on a clear day. The distance between the SIJ and the church was calculated by coordinates and it was 3374.11 meters. Then, it was necessary to know the size of the church in order to compare it to the size of the sun. The church, which had a prism shape, was measured at the site and its side length was 5.58 meters. With the data of the sun diameter and its distance to the earth, the size of the sun in the photos could be calculated.

The software Visual Builder was used to measure the size of the church in pixels. The programme recognises the points where there are any changes in the photos, then the lengths between these points can be measured in pixels. The figure 57 shows the points detected by Visual Builder.
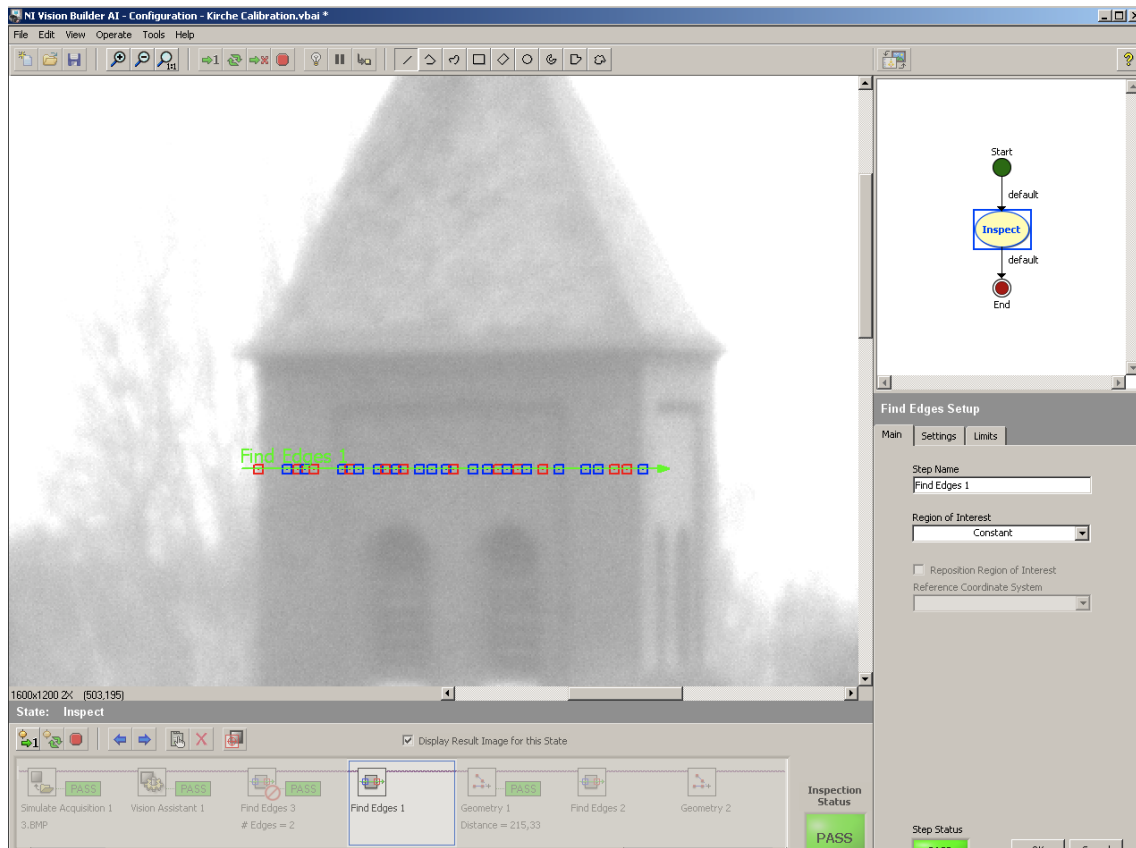
Figure 57: Measurement of the left side of the church.

For the comparison of the size in pixels and metres, the measurements of both sides of the prism were necessary in order to know the angle from which the photos were taken. The figure 58 explains it.
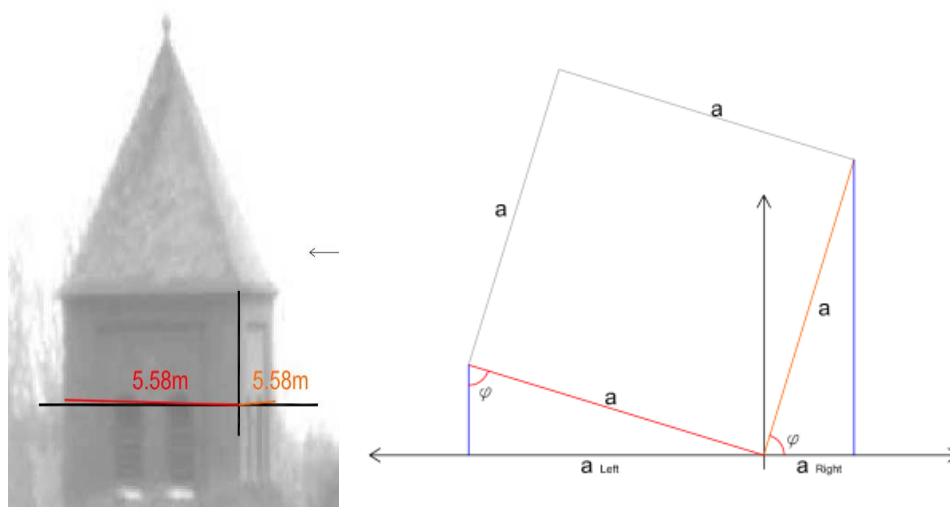

Figure 58: Sides of the church and angles

Analysis of aerosol particles for the determination of energy losses in solar power plants

With the measurements from both sides (left and right), the angle can be calculated with trigonometry. Then, one can calculate the data of the visible side in meters. To obtain this data, the following relations were used:

$\sin\varphi$ = a left / a (1)

$\cos\varphi$ = a right / a (2)

Dividing (1)/(2) φ = arctg a left / a right

a left (metres) = sen φ * a

Equation 12: trigonometry relations

The data 'a' right and left can be calculated knowing the data of the angle. Then it only remains to compare the size of the church in pixels (P_c) with the real size of the church in metres (S_c) and the distance between the camera and the church in metres (D_c) as well. The size of the sun radius (S_s) and the distance between the sun and the earth are also known (D_s), so the size of the sun in pixels (P_d) can be calculated with the following relation:

$$\frac{D_S}{S_S} \cdot P_S = \frac{D_C}{S_C} \cdot P_c \rightarrow P_S = P_c \cdot \frac{D_C}{S_C} \cdot \frac{D_S}{S_S}$$

Equation 13: length relations

The data of the sun radius is about 6.96 E9 m, and its distance to the Earth in December - January (the orbit is elliptical) is about 1.4710556 E11 m. This distance is called periapsis and it is the closest the earth and the sun can be. According to the estimations of scientists, the periapsis is on the 4th of January. The measurements for this thesis were taken between December 16th and January 13th, and the distance to the sun in these days should be very similar to the periapsis, therefore this length was used.

In the table 19, one can observe the data and the final results of the measurements taken in order to calculate the sun radius in the photos. Three different measurements were taken, so that a better result would be obtained.

Constant data	
Sun radius	6.96 E9 m
Distance earth-sun	1.4710556 E11 m

Distance camera-church	3374.11 m
Church side	5.58 m
First measurement	
Right side measured	42.92 pixels
Left side measured	214.98 pixels
Angle obtained	78.7 °
Left side obtained	5.859 meters
Sun radius obtained	614.04 pixels
Second measurement	
Right side measured	42.02 pixels
Left side measured	214.62 pixels
Angle obtained	78.92 °
Left side obtained	5.593 meters
Sun radius obtained	612.63 pixels
Third measurement	
Right side measured	41.58 pixels
Left side measured	215.33 pixels
Angle obtained	79.07 °
Left side obtained	5.5966 meters
Sun radius obtained	614.21 pixels
Sun radius average	613.63 pixels

Table 19: results of the measurements

Once the sun size has been calculated, the sun radiation in the whole circumsolar area needs to be measured. With the devices used, it was not possible to calculate the exact incoming solar radiation from the different points. It was, however, possible to distinguish it due to the different intensity of the light in the circumsolar area. The variation of the solar radiation is thus determined by its brightness. The following equations were used to calculate the CSR:

$$CSR = \frac{\Phi\,cs}{\Phi\,i}$$

Equation 14: CSR equation

Analysis of aerosol particles for the determination of energy losses in solar power plants

$$\Phi_{i,cs} = 2\pi \int_{0,\theta_\delta}^{\theta_\Delta} \phi(\theta) \sin(\theta) d\theta$$

Equation 15: intensity of the circumsolar area or the solar circle.

The difference between these equations and the equation 15 in the third chapter of the thesis is that the flux is considered as brightness per area instead of sun radiation.

In the pictures taken, one can observe the decreasing intensity at the border of the sun. This variation could be measured with the software Visual Builder. In the figure 59, one can see one of the photos used for the measurements in this thesis.

Figure 59: Picture of the sun on January 13th

A programme, which was created for the purpose of previous studies by the SIJ, can measure the light intensity in a picture for different areas. The programme then exports the information to an excel file.

As one can observe in the figure XXX, the largest possible diameter one can obtain in the picture (due to the focus of the tele lens), is the diagonal one. The diagonal diameter has thus been used to measure the variation of the light intensity. The following picture shows the different areas that the programme used to measure the light intensity. It measured the average intensity for each area inside of the green rectangles. One can see that the rectangles are smaller at the edges of the sun circle because it is the most important area.
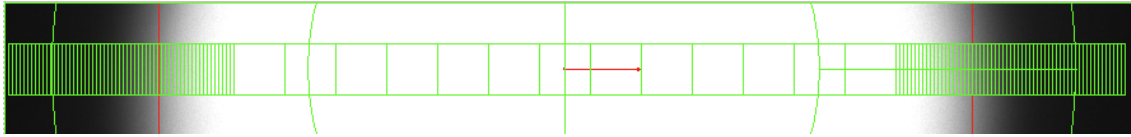
Figure 60: Picture obtained from the software Visual Builder, with which the sun on January 13th 2012 is measured.

The excel file positions every rectangle in the picture, providing all of the distances in pixels.

In order to calculate the estimated circumsolar radiation, it is required to know the brightness of the solar circle and the brightness included into the circumsolar area. Therefore, for the determination of the brightness inside the sun circle, it is necessary to add the flux (area*brightness) inside a circle with a radius of 613,63 pixels. It is further necessary to also add the flux of the circumsolar area. The CSR can then be calculated. The table 20 shows part of the results of the measurement on January 13th. As one can see, it shows the average intensity and the centre of each rectangle.

Intensity	R95	Center.X Position (Pixel)	1699
Intensity	MR95	Average Intensity	107,72916
Intensity	R96	Center.X Position (Pixel)	173
Intensity	MR96	Average Intensity	101,63125
Intensity	R97	Center.X Position (Pixel)	1705
Intensity	MR97	Average Intensity	101,38541
Intensity	R98	Center.X Position (Pixel)	167
Intensity	MR98	Average Intensity	95,08334
Intensity	R99	Center.X Position (Pixel)	1711
Intensity	MR99	Average Intensity	95,25625

Table 20: data obtained from the Visual Builder

All of the calculations necessary to obtain the CSR data, which is specified in the chapter 10 "Measurements", were done with the software Microsoft Office Excel.